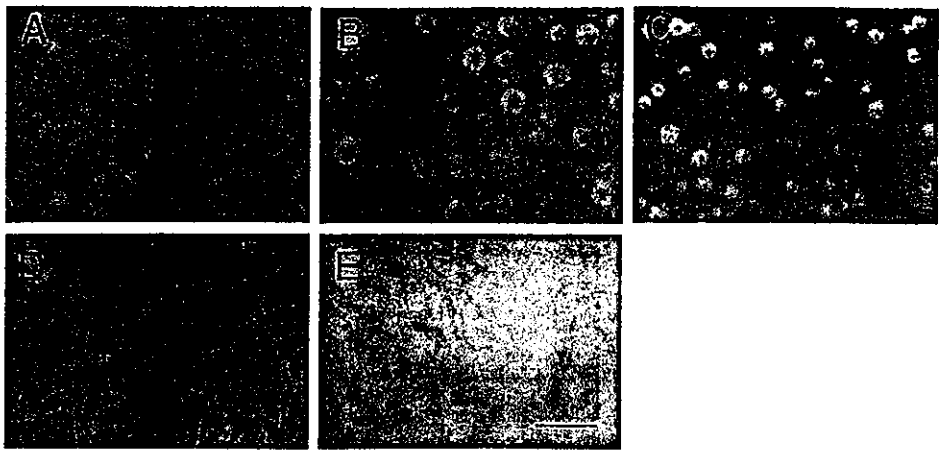

FIG. 1. Phase-contrast micrographs showing isolated germ cells and Sertoli cells from a testicular cell suspension. **A**) Type A spermatogonia. **B**) Spermatocytes. **C**) Spermatids. **D**) Sertoli cells. **E**) Alkaline phosphatase activity of Sertoli cell cultures. Germ cells in **A–C** were from testes of 8-wk-old mice. Sertoli cells in **D** and **E** were from testes of 2-wk-old mice. Scale bar = 30 μm.

from two 8-wk-old adult mice. The purity of each isolated population was <84.5% (Fig. 1A and Table 1). Using phase-contrast microscopy, we determined that these cells were 14–16 μm in diameter. Following elimination of the remaining spermatogonia using magnetic microbeads, the remaining cells were separated into two principal visible bands by centrifugation through a discontinuous Percoll gradient. Phase-contrast microscopy revealed that these two bands consisted primarily of pachytene spermatocytes and round spermatids (Fig. 1, B and C). We isolated an average of 3×10^5 spermatocytes and 200×10^5 spermatids from two 8-wk-old adult mice. We also isolated an average 20×10^5 Sertoli cells from ten 2-wk-old juvenile mice (Fig. 1D). Peritubular myoid cells were identified by alkaline phosphatase staining. Although >95% of these cells were unstained, ~5% of the Sertoli cells showed considerable alkaline phosphatase activity (Fig. 1E).

RT-PCR Analysis of Isolated Cells Expressing Specific Marker Genes

RT-PCR using extracts of isolated cells confirmed the expression of mRNAs from *c-kit,* Histone H1t, *SP-10,* and *SCF.* Each gene was expressed in only one cell type, as follows: *c-kit* in spermatogonia, the Histone H1t gene in spermatocytes, *SP-10* in spermatids, and *SCF* in Sertoli cells (Fig. 2).

Characterization of Isolated Cells by FACS

To determine the purity of isolated germ cells, we used FACS analysis to follow the differentiation-dependent acquisition of stage-specific patterns during spermatogenesis and monitored the percentage of cells with differing DNA content. The histogram in Figure 3 presents the number of cells at each fluorescence level (FL2-A). Diploid (2n DNA) cells were observed in 84.5% of the isolated spermatogonia, tetraploid (4n DNA) cells were observed in 79.6% of the isolated spermatocytes, and haploid (1n DNA) cells were observed in 85.3% of the isolated spermatids (Table 1). These results demonstrate that the majority of cells in each population exhibited the expected ploidy.

TABLE 1. The percentage of 1n, 2n, and 4n cells in isolated germ cells from a testicular cell suspension from 8-wk-old mice, as determined by FACS.[a]

Ploidy[b]	Total cells (%)[c]	Isolated germ cells (%)		
		Spermatogonia	Spermatocytes	Spermatids
1n	56.2 ± 4.2	9.4 ± 1.2	5.3 ± 1.8	85.3 ± 3.3
2n	25.2 ± 3.6	84.5 ± 2.7	9.3 ± 1.3	6.2 ± 0.9
4n	18.6 ± 3.1	12.7 ± 0.9	79.6 ± 2.5	7.7 ± 2.2

[a] Calculated after eliminating cell debris (FL2-A < 50 in Fig. 2).
[b] 1n, haploid cells (one copy of genome); 2n, diploid cells (two copies of genome); 4n, tetraploid cells (four copies of genome).
[c] Each percentage represents the mean ± SD of 4–6 measurements.

Expression of UCH Isozymes During Spermatogenesis

We characterized the expression pattern of each UCH gene in isolated testicular cell populations during spermatogenesis using SYBR Green-based real-time quantitative RT-PCR (Fig. 4). The 2^{-ddCt} values indicate the relative mRNA expression levels compared with spermatogonia from 2-wk-old mice (Sg2). The genes encoding UCH-L1 and UCH-L4 were expressed mainly in spermatogonia (Fig. 4, A and C). UCH-L1 was also expressed significantly in the Sertoli population, and UCH-L4 was expressed to a lesser degree in spermatocytes and spermatids. UCH-L3 and UCH-L5 genes were expressed primarily in the spermatid population and to a much lesser extent in spermatocytes (Fig. 4, B and D). We further examined the expression of UCH mRNAs during testicular maturation (Fig. 5A) in whole testes from 5-, 7-, 15-, 19-, 21-, 23-, 26-, and 33-

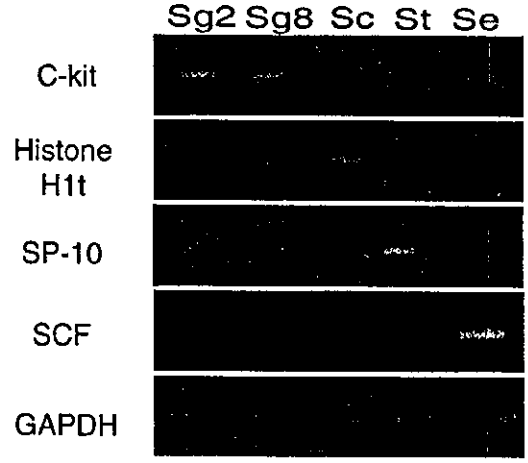

FIG. 2. Expression of c-kit, Histone H1t, SP-10, and SCF mRNAs determined by RT-PCR of extracts of isolated germ cells and Sertoli cells from a testicular cell suspension. Sg2, Spermatogonia of 2-wk-old mice; Sg8, spermatogonia from 8-wk-old mice; Sc, spermatocytes from 8-wk-old mice; St, spermatids from 8-wk-old mice; Se, Sertoli cells from 2-wk-old mice.

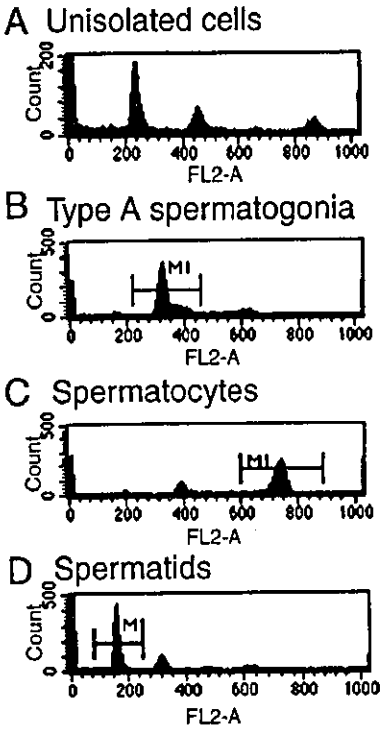

FIG. 3. FACS analysis of isolated germ cells from a testicular cell suspension obtained from 8-wk-old mice. Each window is a histogram representing the number of cells at each fluorescence level (FL2-A). A) Unisolated cells. B) Type A spermatogonia. C) Spermatocytes. D) Spermatids.

day-old mice. The UCH-L1 and UCH-L4 mRNAs were expressed similarly during development and likewise for the UCH-L3 and UCH-L5 genes. The expression of UCH-L1 mRNA appears relatively high on Postnatal Day 15. However, the percentage of spermatogonia and Sertoli cells would have become diluted by meiotic and postmeiotic germ cells after Day 15, thereby accounting for the relatively lower levels of UCH-L1 at subsequent time points. RT-PCR data suggest that UCH-L1 mRNA expression in spermatogonia and Sertoli cells increased continuously even after Postnatal Day 15 (Fig. 5B). We also analyzed the protein expression patterns of UCH-L1 and UCH-L3 in the mouse testis using peptide-specific antibodies that recognize regions in mouse UCH-L1 or UCH-L3. Western blot analysis detected UCH-L1 in spermatogonia and Sertoli cells, and UCH-L3 was detected primarily in spermatocytes and spermatids, as expected, although it was also found to a lesser extent in spermatogonia (Fig. 6A). Also, UCH-L3 expression increased in a differentiation-dependent manner during juvenile spermatogenesis (Fig. 5C). Immunohistochemistry detected homogeneous UCH-L1 expression in both spermatogonia and Sertoli cells from wild-type (Balb/c) and *Uchl3* knockout mice, whereas UCH-L3 was detected mainly in spermatocytes and round spermatids of wild-type (Balb/c) and *gad* mice (Fig. 6, B and C).

DISCUSSION

The ubiquitin pathway plays critical roles in the progression of spermatogenesis through the mitotic, meiotic, and postmeiotic phases [2, 3, 18, 36]. Because numerous proteins are regulated by ubiquitination, mutations that affect the ubiquitin pathway result in the dysregulation of multiple cellular processes and induce apoptosis during spermatogenesis [3, 37–39]. For example, mutation of HR6B, a ubiquitin-conjugating enzyme, affects both meiosis and postmeiotic germ cell development [40–43].

Ubiquitin C-terminal hydrolases catalyze the hydrolysis of C-terminal esters and amides of ubiquitin. These enzymes are believed to play a key role in processing polyubiquitin and ubiquitylated proteolytic peptides [8]. The genes for at least four UCHs, UCH-L1 and UCH-L3–5, have been identified in the mouse. Although the specificity and function of these isozymes in spermatogenesis remains elusive, each of these enzymes contains conserved residues that are critical for enzymatic activity [8–10, 44, 45]. The predominant mouse isozymes, UCH-L1 and UCH-L3, share 52% amino acid sequence identity [10, 13, 45]. However, UCH-L1 mRNA is selectively expressed in the mouse testis and nervous systems [11], whereas UCH-L3 mRNA is expressed in nearly every tissue tested, with high levels in the testis [13]. Intracellular localization of UCH-L1 was reported to be closely associated with the proliferative activity of spermatogonia and Sertoli cells [15–18]. In contrast, the expression of UCH-L3 has not been examined in the testis. To address this question, we first generated poly-

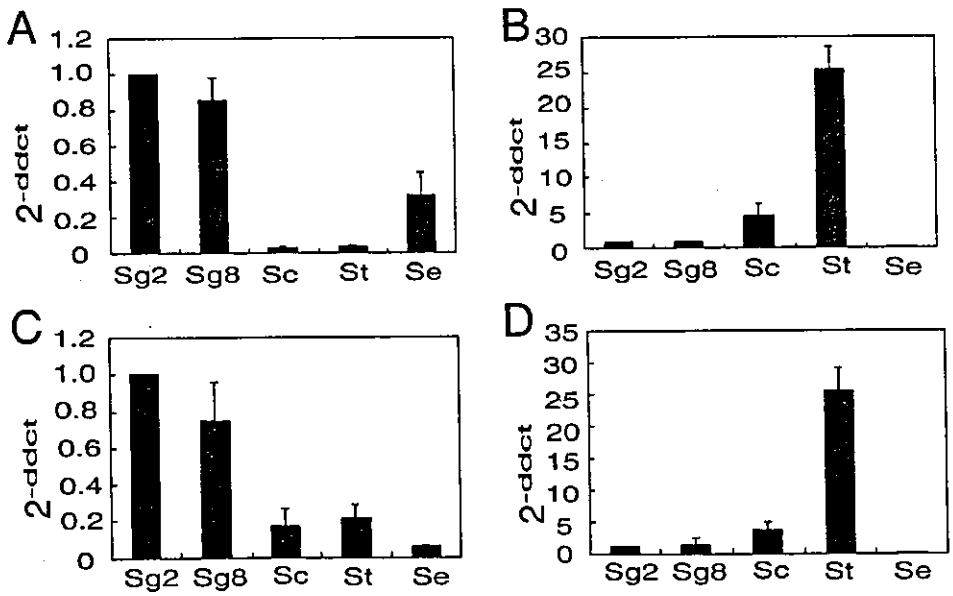

FIG. 4. Comparison of the relative UCH isozyme gene expression levels (2^{-ddCt}) in isolated germ cells and Sertoli cells using RT-PCR. The formula 2^{-ddCt} indicates the relative expression level in isolated testicular cells compared with Sg2 cells. Sg2 gene expression in each case was set to 1.0. A) *Uchl1*. B) *Uchl3*. C) *Uchl4*. D) *Uchl5*. Sg2, Spermatogonia from 2-wk-old mice; Sg8, spermatogonia from 8-wk-old mice; Sc, spermatocytes from 8-wk-old mice; St, spermatids from 8-wk-old mice; Se, Sertoli cells from 2-wk-old mice.

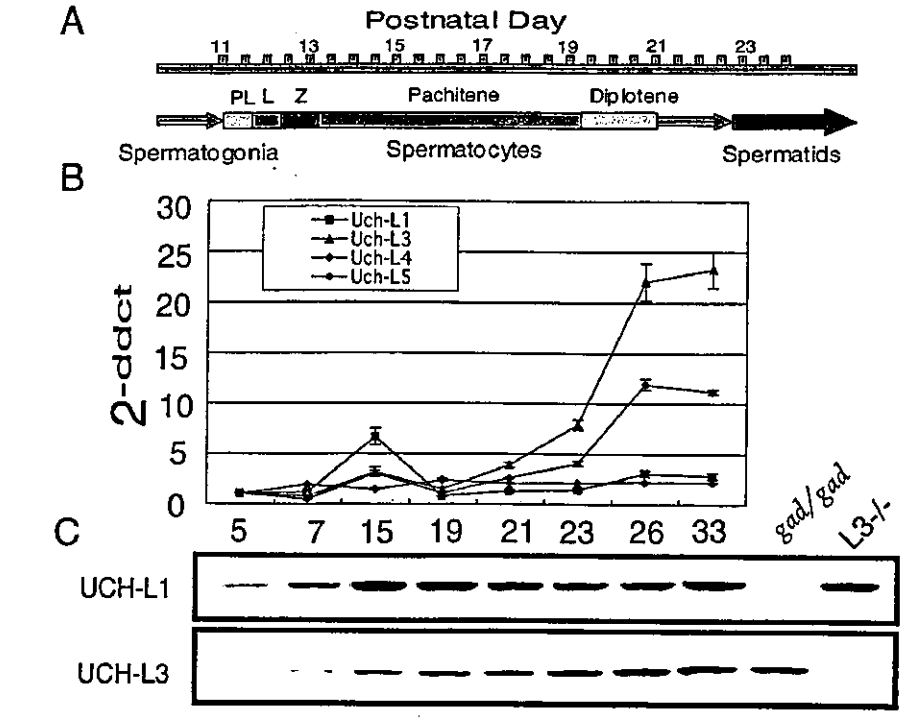

FIG. 5. Expression of UCH isozymes during testicular maturation. A) Timetable for juvenile spermatogenesis. PL, Preleptotene spermatocyte; L, leptotene spermatocyte; Z, zygotene spermatocyte. B) Comparison of the relative UCH isozyme gene expression levels (2^{-ddCt}) by SYBR Green-based real-time quantitative RT-PCR. The value for gene expression from the testes of 5-day-old mice was set to 1.0. C) Comparison of UCH-L1 and UCH-L3 expression by Western blotting. Each lane represents the testes of 5-, 7-, 15-, 19-, 21-, 23-, 26-, or 33-day-old Balb/c mice, *gad* mice, and *Uchl3* knockout mice ($L3^{-/-}$) (**B**, **C**).

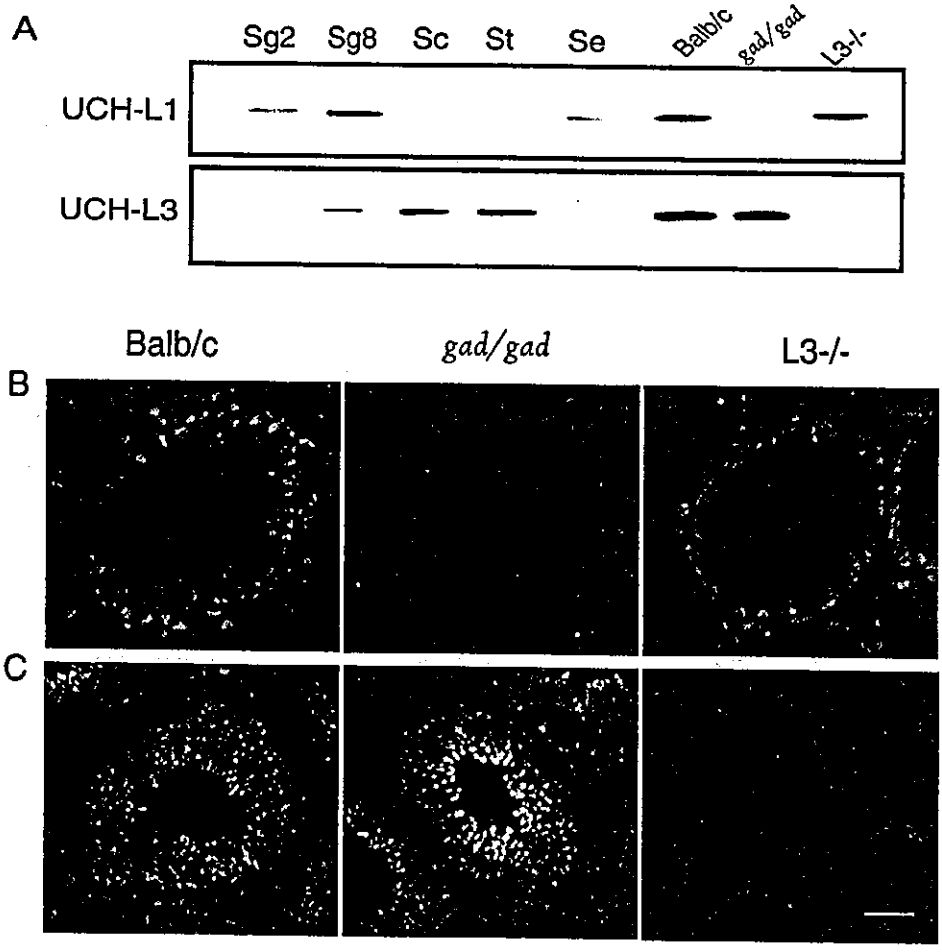

FIG. 6. Analysis of UCH-L1and UCH-L3 expression by western blotting and immunostaining. A) UCH-L1 and UCH-L3 expression in isolated germ cells and Sertoli cells. Sg2, Spermatogonia from 2-wk-old mice; Sg8, spermatogonia from 8-wk-old mice; Sc, spermatocytes from 8-wk-old mice; St, spermatids from 8-wk-old mice; Se, Sertoli cells from 2-wk-old mice. Balb/c, testis from a Balb/c mouse; *gad/gad*, testis from a *gad* mouse (*Uchl1* knockout mouse); $L3^{-/-}$, testis from a *Uchl3* knockout mouse. Immunohistochemistry of UCH-L1 (B) and UCH-L3 (C) in the testis of wild type, *gad*, and *Uchl3* knockout mouse. Stages V–VIII of seminiferous epithelium predominate in each panel as visualized by PAS staining of serial sections. Green fluorescence represents UCH-L1 (B) and UCH-L3 (C); red fluorescence represents staining of cell nuclei by propidium iodide (PI). Magnification, ×200. Scale bar = 30 μm.

clonal antibodies that specifically react with mouse UCH-L3. Using RT-PCR and western blotting, we detected high levels of UCH-L3 mRNA and protein in meiotic pachytene spermatocytes and postmeiotic spermatids during spermatogenesis (Figs. 4B and 6A). These results suggest that UCH-L1 and UCH-L3 may play distinct roles in spermatogenesis, in that UCH-L1 may function in mitotic proliferation, whereas UCH-L3 may function in the meiotic differentiation of spermatocytes into spermatids.

Around Postnatal Day 15, the higher expression of UCH-L1 mRNA suggests that UCH-L1 might have certain functions during testicular maturation. Furthermore, the increased expression of UCH-L1 after Postnatal Day 15 suggests that it might play an active role in mitotic proliferation. In addition to the *Uchl1* genes, we also analyzed transcription from two other UCH isozyme genes, *Uchl3* and *Uchl5,* in isolated testicular cells. UCH-L3 and UCH-L5 mRNAs were found in meiotic pachytene spermatocytes and postmeiotic spermatids (Fig. 4, B and D) and showed similar expression patterns during the course of testicular maturation (Fig. 5B). These results suggest that the *Uchl3* and *Uchl5* genes may have overlapping functions during spermatogenesis. The ubiquitin pathway is very active during the postmitotic phase of spermatogenesis [3, 36]. Thus, UCH-L3 may function to regulate the cell cycle and chromatin structure during the meiotic phase but may facilitate the en masse degradation of cytoplasmic proteins as well as organelle/nuclear remolding during the postmeiotic phase. The present study demonstrates for the first time that UCH-L3 is expressed mainly in meiotic spermatocytes and postmeiotic spermatids during spermatogenesis. Although UCH-L3 shares considerable sequence homology with UCH-L1, the hydrolytic activity of UCH-L3 in vitro differs substantially from that of UCH-L1. The rate of UCH-L3-mediated catalysis (K_{cat}) is more than 200 times greater than UCH-L1 using ubiquitin amide as a substrate [46]. This relatively high activity of UCH-L3 is consistent with its expression during the postmitotic phase of spermatogenesis, in that maturation from spermatocytes to spermatids may be critically dependent on the ubiquitin pathway despite the fact that *Uchl3* knockout mice exhibit normal fertility [13].

In conclusion, our results demonstrate that the expression of UCH isozymes is differentially and developmentally regulated during spermatogenesis and that UCH-L1 and UCH-L3 likely have distinct functions during different developmental phases. These results enhance our understanding of how the ubiquitin pathway is regulated by UCH isozymes during spermatogenesis. Moreover, isolation of mouse germ cells and Sertoli cells from testes may afford the opportunity to assess UCH isozyme function during spermatogenesis in vitro. UCH-L1 has been suggested to associate with monoubiquitin and thereby increase the half-life of ubiquitin in neurons [47]. In addition, a UCH-L1 ubiquityl ligase-like activity has also been proposed [46]. Further biochemical and genetic analyses of UCH family members will help elucidate the role of UCHs in the complex molecular mechanisms involved in spermatogenesis.

REFERENCES

1. Weissman AM. Themes and variations on ubiquitylation. Nat Rev Mol Cell Biol 2001; 2:169–178.
2. Baarends WM, Roest HP, Grootegoed JA. The ubiquitin system in gametogenesis. Mol Cell Endocrinol 1999; 151:5–16.
3. Baarends WM, van der Laan R, Grootegoed JA. Specific aspects of the ubiquitin system in spermatogenesis. J Endocrinol Invest 2000; 23:597–604.
4. Ciechanover A, Orian A, Schwartz AL. Ubiquitin-mediated proteolysis: biological regulation via destruction. Bioessays 2000; 22:442–451.
5. Varshavsky A. The ubiquitin system. Trends Biochem Sci 1997; 22: 383–387.
6. Wilkinson KD. Roles of ubiquitinylation in proteolysis and cellular regulation. Annu Rev Nutr 1995; 15:161–189.
7. Grimes SR, Wilkerson DC, Noss KR, Wolfe SA. Transcriptional control of the testis-specific histone H1t gene. Gene 2003; 304:13–21.
8. Wilkinson KD. Regulation of ubiquitin-dependent processes by deubiquitinating enzymes. FASEB J 1997; 11:1245–1256.
9. Mayer AN, Wilkinson KD. Detection, resolution, and nomenclature of multiple ubiquitin carboxyl-terminal esterases from bovine calf thymus. Biochemistry 1989; 28:166–172.
10. Kurihara LJ, Kikuchi T, Wada K, Tilghman SM. Loss of Uch-L1 and Uch-L3 leads to neurodegeneration, posterior paralysis and dysphagia. Hum Mol Genet 2001; 10:1963–1970.
11. Saigoh K, Wang YL, Suh JG, Yamanishi T, Sakai Y, Kiyosawa H, Harada T, Ichihara N, Wakana S, Kikuchi T, Wada K. Intragenic deletion in the gene encoding ubiquitin carboxy-terminal hydrolase in gad mice. Nat Genet 1999; 23:47–51.
12. Wilkinson KD, Deshpande S, Larsen CN. Comparisons of neuronal (PGP 9.5) and non-neuronal ubiquitin C-terminal hydrolases. Biochem Soc Trans 1992; 20:631–637.
13. Kurihara LJ, Semenova E, Levorse JM, Tilghman SM. Expression and functional analysis of Uch-L3 during mouse development. Mol Cell Biol 2000; 20:2498–2504.
14. Zhang N, Wilkinson K, Bownes M. Cloning and analysis of expression of a ubiquitin carboxyl terminal hydrolase expressed during oogenesis in *Drosophila melanogaster.* Dev Biol 1993; 157:214–223.
15. Wilson PO, Barber PC, Hamid QA, Power BF, Dhillon AP, Rode J, Day IN, Thompson RJ, Polak JM. The immunolocalization of protein gene product 9.5 using rabbit polyclonal and mouse monoclonal antibodies. Br J Exp Pathol 1988; 69:91–104.
16. Tokunaga Y, Imai S, Torii R, Maeda T. Cytoplasmic liberation of protein gene product 9.5 during the seasonal regulation of spermatogenesis in the monkey (*Macaca fuscata*). Endocrinology 1999; 140: 1875–1883.
17. Kon Y, Endoh D, Iwanaga T. Expression of protein gene product 9.5, a neuronal ubiquitin C-terminal hydrolase, and its developing change in Sertoli cells of mouse testis. Mol Reprod Dev 1999; 54:333–341.
18. Kwon J, Kikuchi T, Setsuie R, Ishii Y, Kyuwa S, Yoshikawa Y. Characterization of the testis in congenitally ubiquitin carboxy-terminal hydrolase-1 (Uch-L1) defective (gad) mice. Exp Anim 2003; 52:1–9.
19. Loveland KL, Schlatt S. Stem cell factor and c-kit in the mammalian testis: lessons originating from mother nature's gene knockouts. J Endocrinol 1997; 153:337–344.
20. Lassalle B, Ziyyat A, Testart J, Finaz C, Lefevre A. Flow cytometric method to isolate round spermatids from mouse testis. Hum Reprod 1999; 14:388–394.
21. van der Wee KS, Johnson EW, Dirami G, Dym TM, Hofmann MC. Immunomagnetic isolation and long-term culture of mouse type A spermatogonia. J Androl 2001; 22:696–704.
22. van Pelt AM, Morena AR, van Dissel-Emiliani FM, Boitani C, Gaemers IC, de Rooij DG, Stefanini M. Isolation of the synchronized A spermatogonia from adult vitamin A-deficient rat testes. Biol Reprod 1996; 55:439–444.
23. von Schonfeldt V, Krishnamurthy H, Foppiani L, Schlatt S. Magnetic cell sorting is a fast and effective method of enriching viable spermatogonia from Djungarian hamster, mouse, and marmoset monkey testes. Biol Reprod 1999; 61:582–589.
24. Kato S, Kobayashi T, Kusuda K, Nishina Y, Nishimune Y, Yomogida K, Yamamoto M, Sakagami H, Kondo H, Ohnishi M, Chida N, Yanagawa Y, Tamura S. Differentiation-dependent enhanced expression of protein phosphatase 2Cbeta in germ cells of mouse seminiferous tubules. FEBS Lett 1996; 396:293–297.
25. Anthony CT, Skinner MK. Cytochemical and biochemical characterization of testicular peritubular myoid cells. Biol Reprod 1989; 40: 811–823.
26. Scarpino S, Morena AR, Petersen C, Froysa B, Soder O, Boitani C. A rapid method of Sertoli cell isolation by DSA lectin, allowing mitotic analyses. Mol Cell Endocrinol 1998; 146:121–127.
27. Cox WG, Singer VL. A high-resolution, fluorescence-based method for localization of endogenous alkaline phosphatase activity. J Histochem Cytochem 1999; 47:1443–1456.

28. Bellve AR. Purification, culture, and fractionation of spermatogenic cells. Methods Enzymol 1993; 225:84–113.
29. Malkov M, Fisher Y, Don J. Developmental schedule of the postnatal rat testis determined by flow cytometry. Biol Reprod 1998; 59:84–92.
30. Sorrentino V, Giorgi M, Geremia R, Besmer P, Rossi P. Expression of the c-kit proto-oncogene in the murine male germ cells. Oncogene 1991; 6:149–151.
31. Kurth BE, Wright RM, Flickinger CJ, Herr JC. Stage-specific detection of mRNA for the sperm antigen SP-10 in human testes. Anat Rec 1993; 236:619–625.
32. Mauduit C, Hamamah S, Benahmed M. Stem cell factor/c-kit system in spermatogenesis. Hum Reprod Update 1999; 5:535–545.
33. Aoki K, Sun YJ, Aoki S, Wada K, Wada E. Cloning, expression, and mapping of a gene that is upregulated in adipose tissue of mice deficient in bombesin receptor subtype-3. Biochem Biophys Res Commun 2002; 290:1282–1288.
34. Janca FC, Jost LK, Evenson DP. Mouse testicular and sperm cell development characterized from birth to adulthood by dual parameter flow cytometry. Biol Reprod 1986; 34:613–623.
35. Aoki S, Su Q, Li H, Nishikawa K, Ayukawa K, Hara Y, Namikawa K, Kiryu-Seo S, Kiyama H, Wada K. Identification of an axotomy-induced glycosylated protein, AIGP1, possibly involved in cell death triggered by endoplasmic reticulum-Golgi stress. J Neurosci 2002; 22: 10751–10760.
36. Sutovsky P. Ubiquitin-dependent proteolysis in mammalian spermatogenesis, fertilization, and sperm quality control: killing three birds with one stone. Microsc Res Tech 2003; 61:88–102.
37. Wing SS. Deubiquitinating enzymes—the importance of driving in reverse along the ubiquitin-proteasome pathway. Int J Biochem Cell Biol 2003; 35:590–605.
38. Guardavaccaro D, Kudo Y, Boulaire J, Barchi M, Busino L, Donzelli M, Margottin-Goguet F, Jackson PK, Yamasaki L, Pagano M. Control of meiotic and mitotic progression by the F box protein beta-Trcp1 in vivo. Dev Cell 2003; 4:799–812.
39. van Baren MJ, van der Linde HC, Breedveld GJ, Baarends WM, Rizzu P, de Graaff E, Oostra BA, Heutink P. A double RING-H2 domain in RNF32, a gene expressed during sperm formation. Biochem Biophys Res Commun 2002; 292:58–65.
40. Escalier D, Bai XY, Silvius D, Xu PX, Xu X. Spermatid nuclear and sperm periaxonemal anomalies in the mouse Ube2b null mutant. Mol Reprod Dev 2003; 65:298–308.
41. Baarends WM, Wassenaar E, Hoogerbrugge JW, van Cappellen G, Roest HP, Vreeburg J, Ooms M, Hoeijmakers JH, Grootegoed JA. Loss of HR6B ubiquitin-conjugating activity results in damaged synaptonemal complex structure and increased crossing-over frequency during the male meiotic prophase. Mol Cell Biol 2003; 23:1151–1162.
42. Roest HP, van Klaveren J, de Wit J, van Gurp CG, Koken MH, Vermey M, van Roijen JH, Hoogerbrugge JW, Vreeburg JT, Baarends WM, Bootsma D, Grootegoed JA, Hoeijmakers JH. Inactivation of the HR6B ubiquitin-conjugating DNA repair enzyme in mice causes male sterility associated with chromatin modification. Cell 1996; 86: 799–810.
43. Escalier D. New insights into the assembly of the periaxonemal structures in mammalian spermatozoa. Biol Reprod 2003; 69:373–378.
44. Hershko A, Ciechanover A. The ubiquitin system for protein degradation. Annu Rev Biochem 1992; 61:761–807.
45. Osawa Y, Wang YL, Osaka H, Aoki S, Wada K. Cloning, expression, and mapping of a mouse gene, Uchl4, highly homologous to human and mouse Uchl3. Biochem Biophys Res Commun 2001; 283:627–633.
46. Liu Y, Fallon L, Lashuel HA, Liu Z, Lansbury PT Jr. The UCH-L1 gene encodes two opposing enzymatic activities that affect alpha-synuclein degradation and Parkinson's disease susceptibility. Cell 2002; 111:209–218.
47. Osaka H, Wang YL, Takada K, Takizawa S, Setsuie R, Li H, Sato Y, Nishikawa K, Sun YJ, Sakurai M, Harada T, Hara Y, Kimura I, Chiba S, Namikawa K, Kiyama H, Noda M, Aoki S, Wada K. Ubiquitin carboxy-terminal hydrolase L1 binds to and stabilizes monoubiquitin in neuron. Hum Mol Genet 2003; 12:1945–1958.

Available online at www.sciencedirect.com
SCIENCE DIRECT
Brain Research 1019 (2004) 1–9
BRAIN RESEARCH
www.elsevier.com/locate/brainres

Research report

Accumulation of β- and γ-synucleins in the ubiquitin carboxyl-terminal hydrolase L1-deficient *gad* mouse

Yu-Lai Wang[a], Ayako Takeda[a], Hitoshi Osaka[a,b], Yoko Hara[a], Akiko Furuta[a], Rieko Setsuie[a,c], Ying-Jie Sun[a], Jungkee Kwon[a,d], Yae Sato[a,c], Mikako Sakurai[a,c], Mami Noda[c], Yasuhiro Yoshikawa[d], Keiji Wada[a,*]

[a] *Department of Degenerative Neurological Diseases, National Institute of Neuroscience, National Center of Neurology and Psychiatry, Kodaira, Tokyo 187-8502, Japan*
[b] *Information and Cellular Function, PRESTO, Japan Science and Technology Agency (JST), Kawaguchi, Saitama 332-0012, Japan*
[c] *Laboratory of Pathophysiology, Graduate School of Pharmaceutical Sciences, Kyushu University, Higashi, Fukuoka, 812-8582, Japan*
[d] *Department of Biomedical Science, Graduate School of Agricultural and Life Sciences, University of Tokyo, 1-1-1 Yayoi, Bunkyo, Tokyo, 113-8657, Japan*

Accepted 11 May 2004

Abstract

The synuclein family includes three isoforms, termed α, β and γ. α-Synuclein accumulates in various pathological lesions resulting from neurodegenerative disorders including Parkinson's disease (PD), dementia with Lewy bodies (DLB) and multiple system atrophy. However, neither β- nor γ-synuclein has been detected in Lewy bodies, and thus it is unclear whether these isoforms contribute to neurological pathology. In the present study, we used immunohistochemistry to demonstrate accelerated accumulation of β- and γ-synucleins in axonal spheroids in gracile axonal dystrophy (*gad*) mice, which do not express ubiquitin carboxyl-terminal hydrolase L1 (UCH-L1). γ-Synuclein immunoreactivity in the spheroids appeared in the gracile nucleus at 3 weeks of age and was maintained until 32 weeks. β-Synuclein immunoreactivity appeared in spheroids around 12 weeks of age. In contrast, α-synuclein immunoreactivity was barely detectable in spheroids. Immunoreactivity for synaptophysin and ubiquitin were either faint or undetectable in spheroids. Given that UCH-L1 deficiency results in axonal degeneration and spheroid formation, our findings suggest that β- and γ-synuclein participate in the pathogenesis of axonal swelling in *gad* mice.

Theme: Disorders of the nervous system
Topic: Degenerative disease: other

Keywords: Synuclein; Spheroid; UCH-L1; Ubiquitin

1. Introduction

The synucleins are a family of small cytosolic proteins that are expressed abundantly in the nervous system. Their contribution to neurophysiological function, however, is poorly understood. The mouse synuclein family consists of three members, α-synuclein (α-syn), β-synuclein (β-syn) and γ-synuclein (γ-syn), which range from 123 to 140 residues in length, exhibit 48–58% amino acid sequence identity and share similar domain organization (Fig. 1). Immunohistochemistry in the normal brain shows that α- and β-syn are concentrated at nerve terminals with little staining of somata and dendrites. Ultrastructural studies show that these isoforms localize to nerve terminals in close proximity to synaptic vesicles [18]. In contrast, γ-syn is present throughout nerve cells and is most abundant in the peripheral nervous system [5,18].

The synuclein family has been implicated in neurodegenerative diseases. Two point mutations (A53T, A30P) in the gene encoding α-synuclein (*SNCA*) have been detected in two distinct Parkinson's disease (PD) sibships with autosomal dominant inheritance [17,26], and a heritable

* Corresponding author. Tel.: +81-42-346-1715; fax: +81-42-346-1745.
E-mail address: wada@ncnp.go.jp (K. Wada).

0006-8993/$ - see front matter © 2004 Elsevier B.V. All rights reserved.
doi:10.1016/j.brainres.2004.05.023

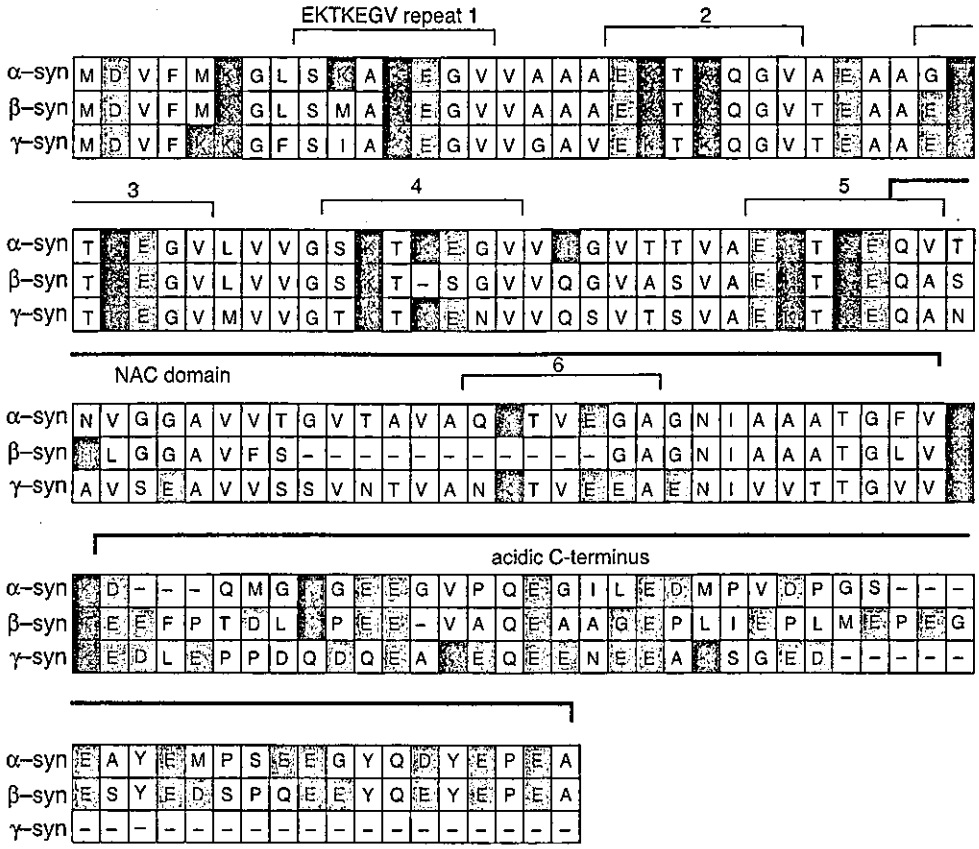

Fig. 1. Comparison of amino acid sequences from mouse α-, β- and γ-synuclein. The N-terminal region contains six imperfect repeats of the consensus EKTKEGV and the C-terminal region is negatively charged. A part of the hydrophobic NAC (non-amyloid component of amyloid plaque) domain is deleted in β-syn. Basic and acidic residues are shown in blue and red, respectively. Sequence accession numbers: mouse α-syn, NP-033247; mouse β-syn, NP-291088; mouse γ-syn, NP-035560.

genomic triplication of *SNCA* has been described within two distinct families [6,33]. Also, α-synuclein protein is a primary component of Lewy bodies (intracellular inclusions) and accumulates in abnormal neurites that contain ubiquitin, synaptophysin and neurofilaments [9,36,37]. β-Syn and γ-syn, which is also known as breast cancer-specific gene 1 (*BCSG1*), are overexpressed in neurodegenerative diseases such as PD and dementia with Lewy bodies (DLB) [5,7]. Unlike α- and β-syn, γ-syn is distributed throughout the cytoplasm of neurons where it influences the integration of neurofilament networks [4].

Ubiquitin carboxyl-terminal hydrolase L1 (UCH-L1) has been found throughout the brain and testis/ovary and has been considered as plays an important role in the labeling of abnormal proteins in the ubiquitin-proteasome system [15,38]. The gracile axonal dystrophy (*gad*) mouse is an autosomal recessive spontaneous mutant that was identified in 1984 [42]. It is the first mammalian neurological model with a defect in the ubiquitin-proteasome system [28]. These mice carry an intragenic deletion of the UCH-L1 gene (*Uchl1*) and do not express UCH-L1, making them comparable to a *Uchl1* null mutant [24,28]. The *gad* mouse exhibits severe sensory ataxia at an early stage, followed by motor paresis at a later stage [14,42]. In the central nervous system of *gad* mice, axonal degeneration begins from the distal ends of primary ascending axons in the dorsal root ganglia (DRG) [21,22]. Spheroid formation with the dying-back type of axonal degeneration is first observed in the gracile and dorsal spinocerebellar tracts [14,21,42]. In the most rostral portion of the gracile fascicles, spheroids are observed around 12 weeks of age and their formation progresses gradually to the terminal stage after 20 weeks of age [22]. At a later stage, axonal degeneration and spheroid formation are observed in the upper tracts of DRG neurons as well as in motor neurons [22]. Although the *gad* mutation is known to be caused by a deficiency in UCH-L1, the mechanism of spheroid formation is not well understood. Dystrophic axons or axonal spheroids have been observed in the brains of patients with infantile neuroaxonal dystrophy [1], in the globus pallidus in Hallervorden-Spatz disease [10], and in the gracile and cuneate nuclei in human vitamin-E deficiency [29]. Furthermore, spheroids are often observed in the medulla and spinal cords of aged mammals. In normal mice, the number of spheroids increases with age in the gracile nucleus [43].

Components of the spheroids of *gad* mice include amyloid-β protein, mitochondria, neurofilaments and synaptic complexes [12,22]. Ubiquitin and amyloid-β protein

also accumulate outside spheroids along the sensory and motor nervous systems [12,40]. We previously observed dot-like deposits of ubiquitin immunoreactivity throughout the gracile nucleus [40]. These data led us to suggest that the absence of functional UCH-L1 may affect the hydrolysis of unknown substrates, which could result in the formation of protein aggregates. α-Syn accumulation has been detected in spheroids resulting from type 1 iron accumulation in the brain (NBIA 1), a rare neurodegenerative disorder characterized by axonal spheroids and Lewy body-like intraneuronal inclusions [8]. Moreover, β-syn and γ-syn immunoreactivity were detected in spheroids but not in Lewy body-like inclusions [8]. In PD and DLB, axonal spheroid-like lesions were identified in the molecular layer of the dentate gyrus along with the accumulation of γ-syn, but not of α- or β-syn [7].

In the present study, we investigated the accumulation of α-syn, β-syn and γ-syn in the *gad* mouse using isoform-specific antibodies. Unexpectedly, we did not detect α-syn in spheroids, although β-syn and γ-syn accumulated in these structures beginning at an early stage of pathology. These results demonstrate that the *gad* mouse constitutes a useful model for investigating the role of synucleins in neurodegeneration.

2. Materials and methods

2.1. Animals

All mice were maintained and propagated at our institute. Adult homozygous *gad/gad* and wild-type (+/+) mice were obtained by mating heterozygous males with heterozygous females. All mouse experiments were performed in accordance with our institution's regulations for animal care and with the approval of the Animal Investigation Committee of the National Institute of Neuroscience, National Center of Neurology and Psychiatry. Each experimental group consisted of three male mice of the same phenotype, and experiments were conducted at 3 weeks (initial stage), 12 weeks (progressive stage), 17 and 20 weeks (critical stage), and 32 weeks (terminal stage) after birth [44].

2.2. Histochemistry

Mice were anesthetized and perfused with 0.9% NaCl followed by ice-cold 4% paraformaldehyde in phosphate-buffered saline (PBS, pH 7.4). Brains and spinal cords were then collected and postfixed in 4% paraformaldehyde overnight at 4 °C. The medulla oblongata and the upper cervical cord were examined. To ensure near complete concordance in the anatomical level of each sample, we followed the Atlas of the Mouse Brain and Spinal Cord [32]. Coronal sections were made at the level of the gracile nucleus (level 535) and of the cervical (C3) spinal cord segments. The samples were embedded in paraffin and sectioned (4 μm) for immunostaining and light microscopy. All sections from mice of the same age group were processed in parallel for each marker. Some sections were stained with hematoxylin–eosin (HE) and Klüver-Barrera for examination by conventional pathological methods. Quantification using stereological techniques was performed by counting eosinophilic spheroids at the medulla and upper cervical levels in at least three sections per sample by two blind observers. We then calculated the average number of spheroids per section. Spheroids were counted using the 200× lens of a Zeiss Axioplan microscope. Under this magnification, eosinophilic spheroids are clearly viewed.

For immunohistochemistry, serial sections were deparaffinized in xylene and graded ethanol, washed in distilled water, and then treated with 0.3% H_2O_2 in methanol for 30 min to quench endogenous peroxidase activity. For the enhancement of α-syn immunostaining, sections were pretreated with 99% formic acid for 5 min or autoclaved at 121 °C for 10 min [35,36]. The sections were washed three times for 5 min in PBS, and then nonspecific binding sites were blocked by incubation in 10% normal serum obtained from the species in which the secondary antibody was generated. After a brief rinse with PBS, sections were incubated overnight at 4 °C with primary antibodies. Primary and secondary antibodies were diluted in DAKO Antibody Diluent (Dako, CA). The following antibodies were used at the final dilutions indicated: monoclonal α-syn antibody (1:100; BD Transduction Laboratories, CA), polyclonal β-syn antibody (1:200; Affinity Research Products), monoclonal synaptophysin antibody (1:50; Dako) and polyclonal ubiquitin antibody (1:400; Chemicon, Temecula). Polyclonal γ-syn antibody (see below) was diluted 1:100.

Subsequent antibody detection was carried out using anti-rabbit or anti-mouse IgG from the VECTASTAIN Elite ABC kit (Vector Labs, Burlingame, CA). Briefly, after washing, sections were sequentially incubated with biotinylated secondary antibodies for 1 h followed by avidin–biotin complex (diluted 1:200) for 1 h. Bound antibody complexes were visualized using 3,3′-diaminobenzidine tetrachloride as a peroxidase substrate. Sections were then lightly counterstained with hematoxylin. For the blocking experiments, anti-γ-syn was initially incubated with recombinant γ-syn for 4 h at 4 °C and the staining procedure was then performed as described above. The sections from different groups were immunostained and treated at the same time. For controls, the primary antibody was replaced with normal rabbit serum or was omitted (these controls always yielded negative staining).

2.3. Preparation of γ-syn antibody and antibody purification

γ-Syn cDNA was cloned from mouse brain mRNA using PCR with a primer set designed using the γ-syn nucleotide

sequence in GenBank (AF017255; sense primer, 5′-ACATGCATGCGACGTCTTCAAGAAAGGCTTC-3′; antisense primer, 5′-CCCAAGCTTGTCTTCTCCACTCTTGGC-3′). The γ-syn cDNA was cloned into the expression vector pEQ-30 (Qiagen, Germany), yielding a recombinant plasmid used to express histidine-tagged γ-syn (6-His-γ-syn) in *E. coli*. Recombinant 6-His-γ-syn was prepared as previously described [23] and used to generate a polyclonal antiserum in rabbits (Takara, Japan). The polyclonal antibodies were purified by affinity chromatography according to the manufacturer's instructions.

2.4. Specificities of synuclein antibodies

Purified recombinant α-syn (BD Transduction Laboratories), β-syn (Alpha Diagnostic International, TX) and γ-syn were diluted and subjected to electrophoresis through SDS-polyacrylamide gels (15% acrylamide) at 200, 100, 50, 25 and 12.5 ng per lane for each protein. The proteins were electrophoretically transferred to PVDF membranes (Bio-Rad, CA) as previously reported [23]. For immunochemical detection of the proteins, the membranes were first blocked in Tris-buffered saline containing 0.1% (w/v) Tween 20 (TTBS) and 3% BSA overnight at 4 °C and then incubated for 12 h with anti-α-syn (1:1000) or with anti-β- or anti-γ-syn (1:500). Antibodies were diluted in DAKO Antibody Diluent. The membranes were washed with TTBS and then incubated with horseradish peroxidase (HRP)-conjugated goat anti-rabbit or anti-mouse IgG (1:10,000; Pierce, IL) for 1 h. Proteins were detected using the SuperSignal chemiluminescence system (Pierce).

3. Results

3.1. Histopathological analysis of the gracile nucleus by HE staining

Oval or round spheroids were visualized by HE staining of axonal sections from wild-type mice at 20 weeks of age. However, fewer than five spheroids per section were detected. In contrast, gracile nuclei of *gad* mice exhibited both axonal dystrophy and spheroids as early as 3 weeks of age (Fig. 2A), in agreement with a previous report [44]. The number of spheroids increased with age, and the HE staining intensity of spheroids was relatively high until 20 weeks of age (Fig. 2B,C) but was very faint at 32 weeks (Fig. 2D). The size and appearance of the spheroids detected in *gad* mice varied with age. Irregularly shaped spheroids were observed from 12 to 20 weeks, whereas other spheroids stained diffusely or granularly as observed in wild-type mice (Fig. 2E). Some spheroids displayed an intense eosinophilic core, vacuoles or thin clefts (Fig. 2B).

We manually counted the total number of spheroids in the dorsal columns and dorsal nuclei of the medulla and upper cervical spinal cord using stereological techniques. Spheroids were detected in *gad* mice at all ages examined (Fig. 2F). The number of spheroids increased with age until 20 weeks (mean ± S.D.; $n = 8 \sim 13$): 3 weeks, 3.2 ± 0.8; 12 weeks, 12.1 ± 3.4; 20 weeks, 16.3 ± 3.9. At 32 weeks, however, the number of spheroids decreased (7.8 ± 2.2), as did their size (data not shown). These observations most likely reflect the severity of degeneration following the progression of the dying-back type of axonal dystrophy [14,44] to the lower spinal cord. In comparison, only a very

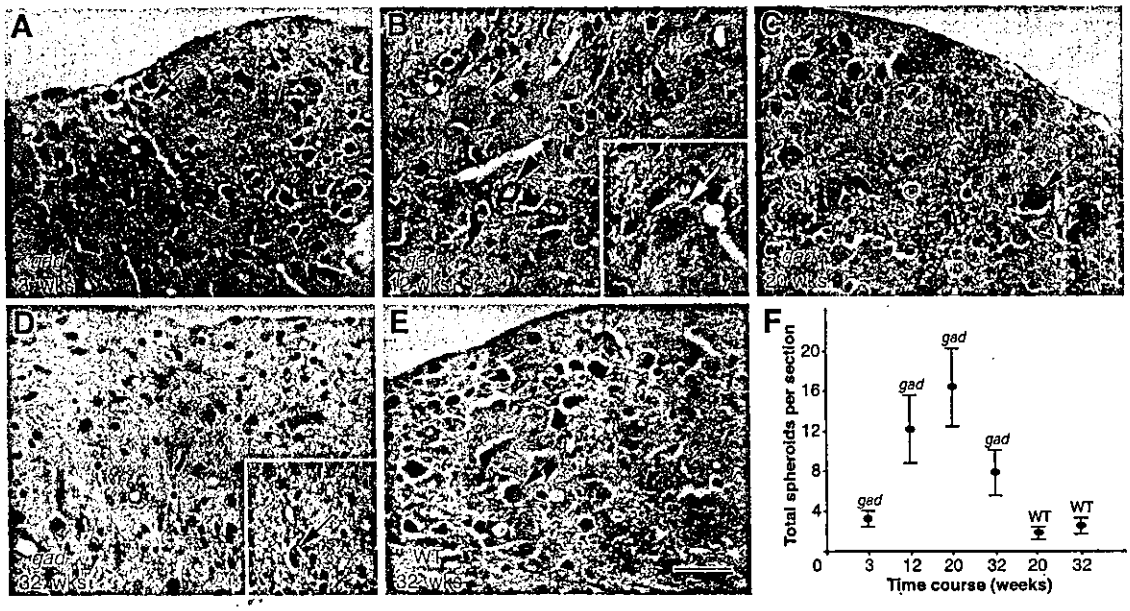

Fig. 2. Hematoxylin–eosin staining of eosinophilic spheroids (arrows) in (A–D) gad sections of the gracile nucleus of the medulla oblongata at 3, 12, 20 and 32 weeks of age, respectively, and in (E) a wild-type section at 32 weeks. An arrowhead indicates a vacuolar spheroid body, and a white arrow indicates a spheroid with an intense eosinophilic core (inset in B). (F) A quantitative study of spheroid number over time in gad and WT mice. Values are the mean ± S.D. ($n = 8 \sim 13$). Bar = 50 μm.

small number of spheroids were found in wild-type mice (1.8±0.6 at 20 weeks, 2.5 ± 0.8 at 32 weeks; $n=9$; Fig. 2F).

3.2. Spheroids of gad mice accumulate β-syn and γ-syn but lack α-syn

We tested the specificity of the synuclein antibodies using purified recombinant synuclein isoforms. Polyclonal anti-γ-syn recognized purified recombinant γ-syn but did not cross-react with recombinant α-syn or β-syn in western blots (Fig. 3C). This antibody was also useful for immunohistochemical detection of γ-syn in spheroids in the gracile nucleus (Fig. 4A–D). No staining was observed when polyclonal anti-γ-syn was pre-absorbed with recombinant γ-syn (1:20 antibody/protein molar ratio; data not shown), thereby demonstrating the specificity of the staining. Under the same conditions, controls without anti-γ-syn showed no immunoreactivity (data not shown). An assay of specificity was also performed using the commercial antibodies against α-syn and β-syn, and similar results were obtained for both antibodies (Fig. 3A,B).

We then utilized all three isoform-specific antibodies to characterize the pathology of axonal degeneration in the *gad* mouse. Immunoreactivity to γ-syn was robust during postnatal weeks 3 ~ 20 but was weak at week 32 (Table 1). At 3 weeks of age, the spheroids detected by anti-γ-syn were more clearly recognized than those detected by HE staining. γ-Syn-immunoreactive spheroids varied in appearance as shown by HE staining (Fig. 2A–D), and oval or round spheroids were often diffusely or granularly immunostained

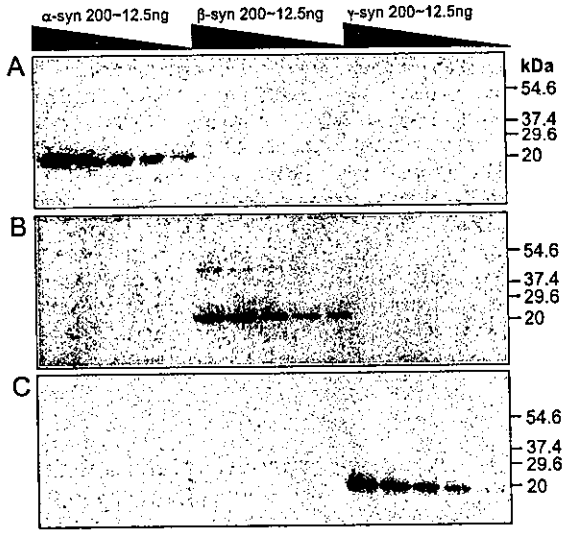

Fig. 3. Specificity of synuclein antibodies. Western blots show the specificity and reactivity of anti-α-syn, anti-β-syn and anti-γ-syn with varying amounts (12.5 ~ 200 ng) of all three recombinant synucleins. Three identical SDS-polyacrylamide gels were transferred to membranes under identical conditions, and each membrane was then probed separately with one of the synuclein antibodies. (A) α-syn antibody. (B) β-syn antibody. (C) γ-syn antibody. None of the antibodies exhibited significant cross-reactivity. A dimer formation (~ 50 kDa) was seen in the β-syn blot (B). Molecular weight markers (in kDa) are shown to the right.

by anti-γ-syn (Fig. 4A–C). Numerous dystrophic axons also displayed γ-syn immunoreactivity. γ-Syn immunoreactivity was absent both in spheroids and dystrophic axons when anti-γ-syn was pre-incubated with excess purified γ-syn (data not shown). In contrast to γ-syn immunoreactivity, spheroids started to exhibit faint and sporadic β-syn immunostaining from 12 weeks of age, with the intensity increasing through 32 weeks (Fig. 4E,F and Table 1). At 32 weeks, relatively intense β-syn staining was observed in spheroids and dystrophic axons (Fig. 4G); however, there were fewer immunopositive spheroids than were seen by γ-syn staining (at 20 weeks; Fig. 4C). Coarse granules around neurons were also immunostained by anti-β-syn (Fig. 4G). Very little α-syn immunoreactivity was observed in spheroids even after enhancement with formic acid or by autoclaving (Fig. 4I). These pretreatments also failed to show α-syn immunoreactivity in axons (Fig. 4I).

In wild-type mice, spheroids were immunopositive for γ-syn (Fig. 4D) and β-syn (a relatively weak punctate pattern in the center of spheroids; Fig. 4H). However, no α-syn immunoreactivity was detected (Fig. 4J, arrows). Also, ubiquitin-positive immunostaining, which did not appear until 20 weeks, was seen in spheroids and as dots that did not correspond to spheroids (data not shown). In *gad* mice, ubiquitin-immunoreactive dots appeared from 12 weeks of age as previously demonstrated [40] and spheroids were not immunoreactive for ubiquitin (Fig. 4K). Ubiquitin staining in general was more intense in the wild-type tissue (Fig. 4L) than in *gad* tissue (Fig. 4K). For synaptophysin, the limited number of spheroids were immunopositive in both wild-type and *gad* mice at 20 weeks of age, with a diffuse or spotty staining in the center of the spheroids (Fig. 4M,O). The *gad* mouse appears to show higher synaptophysin expression than wild-type mice (Fig. 4M,O). At 32 weeks, *gad* mice displayed a punctate distribution pattern of synaptophysin along synapses or surrounding cell bodies with a few densely stained spheroids (Fig. 4N, arrow). In contrast, wild-type mice displayed an expression pattern that was enriched in the spheroids at 32 weeks of age (Fig. 4P, arrow). Furthermore, *gad* mice exhibited dot-like immunostaining for ubiquitin (Fig. 4L, arrowheads), β-syn (Fig. 4G) and γ-syn (Fig. 4C).

4. Discussion

Previous studies of *gad* mice showed axonal degeneration and spheroid-formation (axonal dystrophy) in the gracile tract during the initial stage of neuropathology [14,22,44]. During the critical stage from 17 to 20 weeks of age, the pathological changes extend to the spinocerebellar tract and spinal trigeminal nucleus. During the terminal stage (beyond 32 weeks), these changes extend to the corticospinal tract, cuneate tract, spinal trigeminal tract and thalamus [44]. Although synucleins have been implicated in the pathology of various neurodegenerative disorders, the

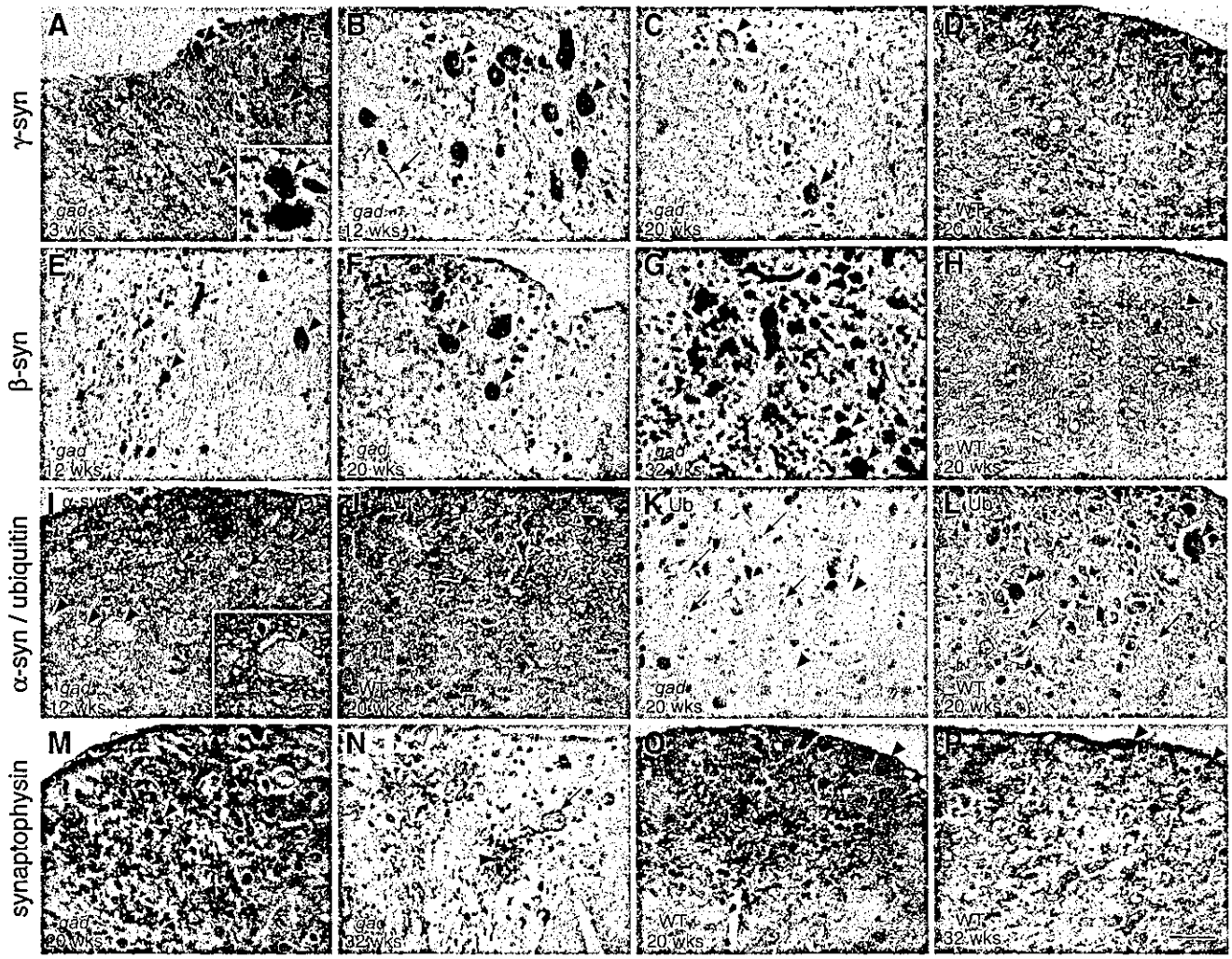

Fig. 4. Synucleins, synaptophysin and ubiquitin immunoreactivities of the gracile nucleus. Almost all spheroids showed strong immunostaining for (A–C) γ-syn and (E–G) β-syn in the gracile nucleus of gad mice from 3 to 32 weeks of age (A, 3 weeks; B and E, 12 weeks; C and F, 20 weeks; G, 32 weeks). Numerous γ-syn-positive spheroids (B, arrowheads) and occasional neurites (B, arrow) are demonstrated. Spheroids from wild-type mice at 20 weeks were also immunopositive for (D) γ-syn (arrowheads) and (H) β-syn (arrowhead). (I) Very little α-syn immunoreactivity was observed in *gad* mouse spheroids (12 weeks, arrowheads). (J) Also, as a positive control, there are any synaptic regions that could be indicated as being positive of α-syn in wild-type mouse (arrows) as well as in gad mouse (I, arrows), but α-syn was not detected in wild-type mouse spheroids (20 weeks, arrowheads). (K) Ubiquitin immunoreactivity in the *gad* mouse gracile nucleus (20 weeks) appeared in dots (arrows) but was not apparent in spheroids (arrowheads). (L) Ubiquitin-positive immunoreactivity was seen in both spheroids (arrowheads) and dots (arrows) in wild-type mice (20 weeks). For synaptophysin, except for the similar immunostaining pattern of synapses, the limited number of spheroids that were immunopositive exhibited diffuse or spotty staining (arrowheads) that was seen only in the center of spheroids at 20 weeks in both (M) *gad* and (0) wild-type mice. Indeed, *gad* mice had more synaptophysin immunoreactivity than did wild-type mice. (N) At 32 weeks, *gad* mice displayed a punctate distribution pattern of synaptophysin along synapses (arrowhead) or surrounding cell bodies, with a few densely stained spheroids (arrow). (P) In contrast, wild-type mice displayed an in situ expression pattern that was enriched in the spheroids at 32 weeks of age (arrowheads). Bar = 50 μm.

possible temporal relationships between spheroid formation and α-, β- and γ-synucleins in the *gad* mouse brain has not yet been proven. Because the *gad* mouse constitutes a neurodegenerative model for the study of spheroid proliferation in axonal termini, we therefore examined spheroid pathology using antibodies directed against α-, β- and γ-syn. Given that dystrophic swollen axons—the primary *gad* lesion observed in the gracile nucleus—result from spheroid proliferation, we quantitated spheroid formation and immunoreactivity in the medulla and upper cervical spinal cord regions over the lifetime of *gad* mice (Fig. 2F and Table 1).

We initially found that γ-syn-positive spheroids were more conspicuous than HE-stained spheroids during the early stage of age, suggesting that γ-syn is more sensitive and specific than HE for detecting spheroid formation in *gad* mice. β-syn was first detected in spheroids 8 weeks later than γ-syn. This result raises the possibility that the mechanism by which β-syn accumulates in spheroids differs from that of γ-syn and that γ-syn may play a more important role in the pathogenesis of the *gad* mutation. A recent study suggested that synucleins may help to regulate proteasome function by modulating 20S proteasome activity in the case

Table 1
Chronological change in the degree of immunoreactivity for spheroids stained for α-, β- and γ-synuclein and ubiquitin in the medulla and upper cervical cord of *gad* mice

	gad 3 weeks	*gad* 12 weeks	*gad* 20 weeks	*gad* 32 weeks	Wild-type 20 weeks	Wild-type 32 weeks
α-syn	−[a]	±	±	±	−	−
β-syn	−	+	++	+++	+	+
γ-syn	++	++	+++	+	+	+
ub-s[b]	−	−	−	−	+	+
ub-d[c]	−	++	+++	+	+	+

[a] Immunoreactivity: +++, strong; ++, moderate; + to ±, weaker to weak; −, not detectable.
[b] Ubiquitin immunoreactivity in the spheroids.
[c] Ubiquitin immunoreactivity in the dot-like structures.

of γ-syn and by affecting the 26S proteasome in the case of β-syn [34]. Thus, the fact that each of these two synucleins exhibits a distinct time course of spheroid accumulation may reflect differences in their metabolic regulation. Furthermore, γ-syn has a very different pattern of localization in neurons as compared with α-syn and β-syn [27].

Antibodies to ubiquitin recognize most spheroids, although it is unclear whether this recognition reflects sequestered free ubiquitin or ubiquitinated proteins [25,39]. Furthermore, the ubiquitinated substrates in spheroids have not been identified. We show here in *gad* mice that ubiquitin is absent from spheroids but is present in dot-like structures, which is consistent with a previous study [40]. Recently, we demonstrated that the loss of functional UCH-L1 leads to a decrease in free ubiquitin in *gad* mice [24]. In contrast, overexpression of UCH-L1 causes an increase in ubiquitin in both cultured cells and mice [24]. Therefore, we suggest that UCH-L1 ensures ubiquitin stability via prolonging the ubiquitin half-life within neurons as an important carrier protein, and loss of functional UCH-L1 may thus lead to inadequate ubiquitination via a decrease in free ubiquitin. Thus, the reduction in ubiquitin might be responsible for the absence of ubiquitin in *gad* mouse spheroids. Ubiquitin is, however, often detected in spheroid bodies during neurodegenerative diseases [2,41]. In addition, an increase in ubiquitin expression was reported in spheroid bodies in the brains of aged monkeys [31]. Despite the presence of ubiquitin in spheroid bodies in these systems, our data indicate that ubiquitination may not be required for the formation of spheroid bodies.

We found that spheroids were positive for both β- and γ-syn but were slight for α-syn in *gad* mice. Lewy bodies in PD and DLB brains are positive for both α-syn [36] and UCH-L1 [20], whereas we did not detect Lewy bodies or Lewy neurites in *gad* mouse brain. These observations suggest that the molecular mechanism of β- and γ-syn accumulation in *gad* spheroids is different from that in Lewy bodies. β-syn inhibits fibril accumulation of α-syn [11]. Thus, early accumulation of β-syn in the spheroids of *gad* mice may inhibit the accumulation of α-syn in spheroids or axon terminals. It remains unclear whether γ-syn has a similar effect on the accumulation of α-syn. Alternatively, fibril formation of α-syn might be affected by the existence of UCH-L1, and lack of UCH-L1 in the *gad* mouse might result in the suppression of α-syn aggregation in vivo. UCH-L1 was reported to have ubiquitin ligase activity that increased the amount of polyubiquitinated α-syn via K63-linked ubiquitination [19]. Other recent studies have shown that UCH-L1 can deubiquitinate polyubiquitinated α-syn with K48-linked ubiquitination [13,30]. Thus, a close relationship between UCH-L1 and α-syn has been implicated. Aggregates of β-syn and γ-syn have been found in dystrophic neurites associated with PD and other neurodegenerative diseases [7]. Neither protein, however, is detected in Lewy bodies in PD and DLB. Consequently, β-syn and γ-syn pathology may be more specific to spheroid disorders.

Pathological accumulations of β-syn and γ-syn were previously reported in neurological diseases [7]. β-syn is a presynaptic protein and *gad* degeneration starts at the presynapse of the gracile nuclei. Local accumulated β-syn may interfere with other presynaptic proteins in the degenerating terminals. We observed that a presynaptic protein, synaptophysin, was weakly detected in spheroids but strongly expressed in healthy synapses in *gad* mice. This result may support the idea of the effect of locally accumulated β-syn.

Overexpression of γ-syn may influence neurofilament network integrity [4]. Distinct from wild-type mice, in *gad* mice γ-syn immunoreactivity in the spheroids appeared in the gracile nucleus from an early stage, which might contribute to the dysfunction of the nervous system, possibly by interrupting axonal transport. Ubiquitin is known to be transported over long distances via slow axonal transport to synapses [3]. Ubiquitin reduction and the consequent inadequate ubiquitination of proteins may trigger accumulation of proteins that should undergo ubiquitin-dependent degradation. An age-dependent increase in γ- and β-syn-positive spheroids in *gad* mice resembles the accumulation of amyloid-β in spheroids of these mice [12]. Amyloid precursor protein has been shown to be transported by a fast axonal flow [16]. The abnormal accumulation of various proteins at terminals might affect axonal transport from the ganglia, leading to the dying-back type of degeneration of axons with formation of spheroid bodies. The mechanisms involved, however, will require more detailed studies of UCH-L1 and synucleins.

Acknowledgements

We thank Miss S. Kikuchi for assistance in preparation of the sections and Ms. M. Shikama for the care and breeding of animals. This work was supported in part by Grants-in-Aid for Scientific Research from the Ministry of Health, Labour and Welfare of Japan; Grants-in-Aid for Scientific Research from the Ministry of Education, Culture, Sports,

Science and Technology of Japan; a grant from the Organization for Pharmaceutical Safety and Research; and a grant from the Japan Science and Technology Agency.

References

[1] J. Aicardi, P. Castelein, Infantile neuroaxonal dystrophy, Brain 102 (1979) 727–748.

[2] N. Arai, Grumose or foamy spheroid bodies involving astrocytes in the human brain, Neuropathol. Appl. Neurobiol. 21 (1995) 238–245.

[3] A. Bizzi, B. Schaetzle, A. Patton, P. Gambetti, L. Autilio-Gambetti, Axonal transport of two major components of the ubiquitin system: free ubiquitin and ubiquitin carboxyl-terminal hydrolase PGP 9.5, Brain Res. 548 (1991) 292–299.

[4] V.L. Buchman, J. Adu, L.G. Pinon, N.N. Ninkina, A.M. Davies, Persyn, a member of the synuclein family, influences neurofilament network integrity, Nat. Neurosci. 1 (1998) 101–103.

[5] V.L. Buchman, H.J. Hunter, L.G. Pinon, J. Thompson, E.M. Privalova, N.N. Ninkina, A.M. Davies, Persyn, a member of the synuclein family, has a distinct pattern of expression in the developing nervous system, J. Neurosci. 18 (1998) 9335–9341.

[6] M. Farrer, J. Kachergus, L. Forno, S. Lincoln, D.S. Wang, M. Hulihan, D. Maraganore, K. Gwinn-Hardy, Z. Wszolek, D. Dickson, J.W. Langston, Comparison of kindreds with parkinsonism and alpha-synuclein genomic multiplications, Ann. Neurol. 55 (2004) 174–179.

[7] J.E. Galvin, K. Uryu, V.M. Lee, J.Q. Trojanowski, Axon pathology in Parkinson's disease and Lewy body dementia hippocampus contains alpha-, beta-, and gamma-synuclein, Proc. Natl. Acad. Sci. U. S. A. 96 (1999) 13450–13455.

[8] J.E. Galvin, B. Giasson, H.I. Hurtig, V.M. Lee, J.Q. Trojanowski, Neurodegeneration with brain iron accumulation, type 1 is characterized by alpha-, beta-, and gamma-synuclein neuropathology, Am. J. Pathol. 157 (2000) 361–368.

[9] M. Goedert, M.G. Spillantini, Dewy body diseases and multiple system atrophy as alpha-synucleinopathies, Mol. Psychiatry 3 (1998) 462–465.

[10] W. Halliday, The nosology of Hallervorden-spatz disease, J. Neurol. Sci. 134 (1995) 84–91 (Suppl.).

[11] M. Hashimoto, E. Rockenstein, M. Mante, M. Mallory, E. Masliah, beta-synuclein inhibits alpha-synuclein aggregation: a possible role as an anti-parkinsonian factor, Neuron 32 (2001) 213–223.

[12] N. Ichihara, J. Wu, D.H. Chui, K. Yamazaki, T. Wakabayashi, T. Kikuchi, Axonal degeneration promotes abnormal accumulation of amyloid beta-protein in ascending gracile tract of gracile axonal dystrophy (GAD) mouse, Brain Res. 695 (1995) 173–178.

[13] Y. Imai, M. Soda, R. Takahashi, Parkin suppresses unfolded protein stress-induced cell death through its E3 ubiquitin-protein ligase activity, J. Biol. Chem. 275 (2000) 35661–35664.

[14] T. Kikuchi, M. Mukoyama, K. Yamazaki, H. Moriya, Axonal degeneration of ascending sensory neurons in gracile axonal dystrophy mutant mouse, Acta Neuropathol. (Berl.) 80 (1990) 145–151.

[15] Y. Kon, D. Endoh, T. Iwanaga, Expression of protein gene product 9.5, a neuronal ubiquitin C-terminal hydrolase, and its developing change in sertoli cells of mouse testis, Mol. Reprod. Dev. 54 (1999) 333–341.

[16] E.H. Koo, S.S. Sisodia, D.-R. Archer, L.J. Martin, A. Weidemarm, K. Beyreuther, P. Fischer, C.L. Masters, D.L. Price, Precursor of amyloid protein in Alzheimer disease undergoes fast anterograde axonal transport, Proc. Natl. Acad. Sci. U. S. A. 87 (1990) 1561–1565.

[17] R. Kruger, W. Kuhn, T. Muller, D. Woitalla, M. Graeber, S. Kosel, H. Przuntek, J.T. Epplen, L. Schols, O. Riess, Ala30Pro mutation in the gene encoding alpha-synuclein in Parkinson's disease, Nat. Genet. 18 (1998) 106–108.

[18] C. Lavedan, E. Leroy, A. Dehejia, S. Buchholtz, A. Dutra, R.L. Nussbaum, M.H. Polymeropoulos, Identification, localization and characterization of the human gamma-synuclein gene, Hum. Genet. 103 (1998) 106–112.

[19] Y. Liu, L. Fallon, H.A. Lashuel, Z. Liu, P.T. Lansbury Jr., The UCH-L1 gene encodes two opposing enzymatic activities that affect alpha-synuclein degradation and Parkinson's disease susceptibility, Cell 111 (2002) 209–218.

[20] J. Lowe, H. McDermott, M. Landon, R.J. Mayer, K.D. Wilkinson, Ubiquitin carboxyl-terminal hydrolase (PGP 9.5) is selectively present in ubiquitinated inclusion bodies characteristic of human neurodegenerative diseases, J. Pathol. 161 (1990) 153–160.

[21] H. Miura, K. Oda, C. Endo, K. Yamazaki, H. Shibasaki, T. Kikuchi, Progressive degeneration of motor nerve terminals in GAD mutant mouse with hereditary sensory axonopathy, Neuropathol. Appl. Neurobiol. 19 (1993) 41–51.

[22] M. Mukoyama, K. Yamazaki, T. Kikuchi, T. Tomita, Neuropathology of gracile axonal dystrophy (GAD) mouse. An animal model of central distal axonopathy in primary sensory neurons, Acta Neuropathol. (Berl) 79 (1989) 294–299.

[23] K. Nishikawa, H. Li, R. Kawamura, H. Osaka, Y.L. Wang, Y. Hara, T. Hirokawa, Y. Manago, T. Amano, M. Noda, S. Aoki, K. Wada, Alterations of structure and hydrolase activity of parkinsonism-associated human ubiquitin carboxyl-terminal hydrolase L1 variants, Biochem. Biophys. Res. Commun. 304 (2003) 176–183.

[24] H. Osaka, Y.L. Wang, K. Takada, S. Takizawa, R. Setsuie, H. Li, Y. Sato, K. Nishikawa, Y.J. Sun, M. Sakurai, T. Harada, Y. Hara, I. Kimura, S. Chiba, K. Namikawa, H. Kiyama, M. Noda, S. Aoki, K. Wada, Ubiquitin carboxy-terminal hydrolase L1 binds to and stabilizes monoubiquitin in neuron, Hum. Mel. Genet. 12 (2003) 1945–1958.

[25] Y. Oya, H. Nakayasu, N. Fujita, K. Suzuki, Pathological study of mice with total deficiency of sphingolipid activator proteins (SAP knockout mice), Acta Neuropathol. (Berl.) 96 (1998) 29–40.

[26] M.H. Polymeropoulos, C. Lavedan, E. Leroy, S.E. Ide, A. Dehejia, A. Dutra, B. Pike, H. Root, J. Rubenstein, R. Boyer, E.S. Stenroos, S. Chandrasekharappa, A. Athanassiadou, T. Papapetropoulos, W.G. Johnson, A.M. Lazzarini, R.C. Duvoisin, G. Di Iorio, L.I. Golbe, R.L. Nussbaum, Mutation in the alpha-synuclein gene identified in families with Parkinson's disease, Science 276 (1997) 2045–2047.

[27] M.C. Quilty, W.P. Gai, D.L. Pountney, A.K. West, J.C. Vickers, Localization of alpha-, beta-, and gamma-synuclein during neuronal development and alterations associated with the neuronal response to axonal trauma, Exp. Neurol. 182 (2003) 195–207.

[28] K. Saigoh, Y.L. Wang, J.G. Suh, T. Yamanishi, Y. Sakai, H. Kiyosawa, T. Harada, N. Ichihara, S. Wakana, T. Kikuchi, K. Wada, Intragenic deletion in the gene encoding ubiquitin carboxy-terminal hydrolase in gad mice, Nat. Genet. 23 (1999) 47–51.

[29] K. Saito, T. Yokoyama, M. Okaniwa, S. Kamoshita, Neuropathology of chronic vitamin E deficiency in fatal familial intrahepatic cholestasis, Acta Neuropathol. (Berl) 58 (1982) 187–192.

[30] D.M. Sampathu, B.I. Giasson, A.C. Pawlyk, J.Q. Trojanowski, V.M. Lee, Ubiquitination of alpha-synuclein is not required for formation of pathological inclusions in alpha-synucleinopathies, Am. J. Pathol. 163 (2003) 91–100.

[31] C. Schultz, E.J. Dick, A.B. Cox, G.B. Hubbard, E. Braak, H. Braak, Expression of stress proteins alpha B-crystallin, ubiquitin, and hsp27 in pallido-nigral spheroids of aged rhesus monkeys, Neurobiol. Aging 22 (2001) 677–682.

[32] R. Sidman, J.B. Angevine, E.T. Pierce, Atlas of the Mouse Brain and Spinal Cord, Harvard Univ. Press, Cambridge, 1971.

[33] A.B. Singleton, M. Farrer, J. Johnson, A. Singleton, S. Hague, J. Kachergus, M. Hulihan, T. Peuralinna, A. Dutra, R. Nussbaum, S. Lincoln, A. Crawley, M. Hanson, D. Maraganore, C. Adler, M.R. Cookson, M. Muenter, M. Baptista, D. Miller, J. Blancato, J. Hardy, K. Gwinn-Hardy, Alpha-synuclein locus triplication causes Parkinson's disease, Science 302 (2003) 841.

[34] H.M. Synder, K. Mensah, I. Surgucheva, B. Festoff, A. Matouschek, A. Surguchov, B. Wolozin, Effect of alpha, beta and gamma synuclein

on the proteasomal pathways: 20S ubiquitin-independent, 26S ubiquitin-indenedent and 26S ubiquintin-dependent. Program No.132.8. Abstract viewer/Itinerary Planner. Society for Neuroscience, Washinton, DC, 2003.

[35] A. Takeda, M. Mallory, M. Sundsmo, W. Honer, L. Hansen, E. Masliah, Abnormal accumulation of NACP/alpha-synuclein in neurodegenerative disorders, Am. J. Pathol. 152 (1998) 367–372.

[36] A. Takeda, M. Hashimoto, M. Mallory, M. Sundsumo, L. Hansen, E. Masliah, C-terminal alpha-synuclein immunoreactivity in structures other than Lewy bodies in neurodegenerative disorders, Acta Neuropathol. (Berl.) 99 (2000) 296–304.

[37] P.H. Tu, J.E. Galvin, M. Baba, B. Giasson, T. Tomita, S. Leight, S. Nakajo, T. Iwatsubo, J.Q. Trojanowski, V.M. Lee, Glial cytoplasmic inclusions in white matter oligodendrocytes of multiple system atrophy brains contain insoluble alpha-synuclein, Ann. Neurol. 44 (1998) 415–422.

[38] K.D. Wilkinson, S. Deshpande, C.N. Larsen, Comparisons of neuronal (PGP 9.5) and non-neuronal ubiquitin C-terminal hydrolases, Biochem. Soc. Trans. 20 (1992) 631–637.

[39] D. Willwohl, M. Kettner, H. Braak, G.B. Hubbard, E.J. Dick Jr., A.B. Cox, C. Schultz, Pallido-nigral spheroids in nonhuman primates: accumulation of heat shock proteins in astroglial processes, Acta Neuropathol. (Berl) 103 (2002) 276–280.

[40] J. Wu, N. Ichihara, D.H. Chui, K. Yamazaki, T. Kikuchi, Abnormal ubiquitination of dystrophic axons in centralnervous system of gracile axonal dystrophy (gad) mutant mouse, Alzheimer's Res. 47 (1996) 163–168.

[41] T. Yamada, H. Akiyama, P.L. McGeer, Two types of spheroid bodies in the nigral neurons in Parkinson's disease, Can. J. Neurol. Sci. 18 (1991) 287–294.

[42] K. Yamazaki, N. Wakasugi, T. Tomita, T. Kikuchi, M. Mukoyama, K. Ando, Gracile axonal dystrophy (GAD), a new neurological mutant in the mouse, Proc. Soc. Exp. Biol. Med. 187 (1988) 209–215.

[43] K. Yamazaki, H. Moriya, T. Wakabayashi, T. Kikuchi, Substance β-like immunoreactivity in the gracile nucleus and fasciculus in old mice, Neurosci. Lett. 106 (1989) 258–260.

[44] K. Yamazaki, A. Kobayashi, A. Kumazawa, T. Wakabayashi, K. Takeki, Axonal degeneration in the central nervous system of gracile axonal dystroph (gad) mice progresses like in human spinocerebellar ataxias, Biomed. Res. 12 (1991) 143–148.

American Journal of Pathology, Vol. 165, No. 4, October 2004

Cell Injury, Repair, Aging and Apoptosis

Two Closely Related Ubiquitin C-Terminal Hydrolase Isozymes Function as Reciprocal Modulators of Germ Cell Apoptosis in Cryptorchid Testis

Jungkee Kwon,*† Yu-Lai Wang,* Rieko Setsuie,*‡ Satoshi Sekiguchi,† Yae Sato,*‡ Mikako Sakurai,*‡ Mami Noda,‡ Shunsuke Aoki,* Yasuhiro Yoshikawa,† and Keiji Wada*

From the Department of Degenerative Neurological Diseases, National Institute of Neuroscience, National Center of Neurology and Psychiatry, Kodaira, Tokyo; the Department of Biomedical Science,† Graduate School of Agricultural and Life Sciences, University of Tokyo, Tokyo; and the Laboratory of Pathophysiology,‡ Graduate School of Pharmaceutical Sciences, Kyushu University, Fukuoka, Japan*

The experimentally induced cryptorchid mouse model is useful for elucidating the *in vivo* molecular mechanism of germ cell apoptosis. Apoptosis, in general, is thought to be partly regulated by the ubiquitin-proteasome system. Here, we analyzed the function of two closely related members of the ubiquitin C-terminal hydrolase (UCH) family in testicular germ cell apoptosis experimentally induced by cryptorchidism. The two enzymes, UCH-L1 and UCH-L3, deubiquitinate ubiquitin-protein conjugates and control the cellular balance of ubiquitin. The testes of gracile axonal dystrophy (*gad*) mice, which lack UCH-L1, were resistant to cryptorchid stress-related injury and had reduced ubiquitin levels. The level of both anti-apoptotic (Bcl-2 family and XIAP) and prosurvival (pCREB and BDNF) proteins was significantly higher in *gad* mice after cryptorchid stress. In contrast, *Uchl3* knockout mice showed profound testicular atrophy and apoptotic germ cell loss after cryptorchid injury. Ubiquitin level was not significantly different between wild-type and *Uchl3* knockout mice, whereas the levels of Nedd8 and the apoptotic proteins p53, Bax, and caspase3 were elevated in *Uchl3* knockout mice. These results demonstrate that UCH-L1 and UCH-L3 function differentially to regulate the cellular levels of anti-apoptotic, prosurvival, and apoptotic proteins during testicular germ cell apoptosis. *(Am J Pathol 2004, 165:1367–1374)*

In the ubiquitin-proteasome system, the levels of poly- and monoubiquitin are strictly controlled by the balance of two groups of specific enzymes: ubiquitinating enzymes (E1, E2, and E3) and deubiquitinating enzymes (DUBs).[1,2] DUBs are subdivided into ubiquitin C-terminal hydrolases (UCHs) and ubiquitin-specific proteases (UBPs).[3,4] The genes for at least four UCHs, UCH-L1 and UCH-L3, UCH-L4, and UCH-L5, have been identified in mice.[5,6] Among them, UCH-L1 and UCH-L3 predominate; these isozymes have 52% amino acid identity and share significant structural similarity;[7] however, the distribution of these two isozymes is quite distinct in that UCH-L3 mRNA is expressed ubiquitously whereas UCH-L1 mRNA is selectively expressed in the testis/ovary and neuronal cells.[7–10] Despite the high-sequence homology, the *in vitro* hydrolytic activities of these two enzymes differ significantly. The activity (Kcat) of UCH-L3 is more than 200-fold higher than UCH-L1 when a fluorogenic ubiquitin substrate is used.[11] In addition to its relatively weak hydrolase activity, UCH-L1 exhibits dimerization-dependent ubiquityl ligase activity.[11] In contrast, UCH-L3 has little or no ligase activity compared with UCH-L1.[11] It was recently suggested that UCH-L1 has anti-proliferative activity in tumor cells, and that its expression is induced in response to tumor growth.[12] Furthermore, UCH-L1 associates with monoubiquitin and prolongs ubiquitin half-life in neurons.[13] Other work demonstrated that UCH-L3 binds to Nedd8 and subsequently processes its C-terminus.[14] Nedd8 is a small ubiquitin-like protein that shares with ubiquitin the ability to be conjugated to a lysine residue in a substrate protein.[15] Covalent conjugation of proteins by Nedd8 is an important form of the posttranscriptional modification and plays a critical role in many cellular processes.[16] These conju-

Supported by Grants-in-Aid for Scientific Research from the Ministry of Health, Labor, and Welfare of Japan; Grants-in-Aid for Scientific Research from the Ministry of Education, Culture, Sports, Science, and Technology of Japan; a grant from Pharmaceuticals and Medical Devices Agency of Japan; and a grant from Japan Science and Technology Agency.

Accepted for publication June 24, 2004.

Address reprint requests to Keiji Wada, Department of Degenerative Neurological Disease, National Institute of Neuroscience, National Center of Neurology and Psychiatry, Kodaira, Tokyo, 187-8502, Japan. E-mail: wada@ncnp.go.jp.

gates are regulated by a large number of deconjugating enzymes. This activity is unique to UCH-L3 because UCH-L1 is relatively weak to cleave the C terminus of Nedd8.[14–16] Collectively, these data suggest that the two mouse isozymes, UCH-L1 and UCH-L3, have distinct but overlapping functions. In addition, we recently found that *gad* mice, which lack UCH-L1 expression, show reduced retinal cell apoptosis in response to ischemia, suggesting that UCH-L1 may promote apoptosis.[17]

Our previous work focused on the possibility that UCH-L1 and UCH-L3 exhibit functional diversity during spermatogenesis. We showed that both UCH-L1 and UCH-L3 are strongly but reciprocally expressed in the testis during spermatogenesis,[18] suggesting that each isozyme may have a distinct function in the testis. To elucidate the pathophysiological roles of these two isozymes in the testis, our present work examines the extent of heat-induced stress using experimentally induced cryptorchidism in *Uchl3* knockout[7] and *gad* mice.[8] Normally, the testes are maintained in the scrotum at a temperature lower than that of the abdomen. Exposure of a testis to higher body temperature via experimentally induced cryptorchidism results in rapid degeneration of testicular germ cells.[19–22] Recent studies show that testicular germ cell degeneration in cryptorchid testes occurs via apoptosis, and that protein and lipid oxidation, along with p53 promote germ cell death.[23–25] The ubiquitin-proteasome system is required for the subsequent degradation of the damaged testicular germ cells.[26–28] Here, we show that both UCH-L1 and UCH-L3 have reciprocal functions in testicular germ cells during cryptorchid-induced apoptosis. Our data show that the absence of UCH-L1 causes resistance to cryptorchid-induced testicular germ cell apoptosis, and that the knockout of UCH-L3 promotes germ cell apoptosis after cryptorchid injury.

Materials and Methods

Animals

We used 8-week-old *Uchl3* knockout (C57BL/6J)[7,18] and *gad*[8,18,29] (CBA/RFM) male mice. *Uchl3* knockout mice were generated by the standard method using homologously recombinant ES cells, and the knockout line was back-crossed several times to C57BL/6J mice.[7] The *gad* mouse is an autosomal recessive mutant that was obtained by crossing CBA and RFM mice.[8] The *gad* line was maintained by intercrossing for more than 20 generations.[8,29] Both strains were maintained at our institute. Animal care and handling were in accordance with institutional regulations for animal care and were approved by the Animal Investigation Committee of the National Institute of Neuroscience, National Center of Neurology and Psychiatry, Tokyo, Japan.

Unilateral Experimental Cryptorchidism

Unilateral cryptorchidism was experimentally induced under pentobarbital anesthesia (Abbott Laboratories, North Chicago, IL).[20,22] Briefly, a midline abdominal incision was made, and the left testis was displaced from scrotum and fixed to the upper abdominal wall. The right testis remained in the scrotum as an intact control within the same animal. At 0, 4, 7, and 14 days after the operation, four control and four cryptorchid testes were harvested to determine testis weight.

Histological and Immunohistochemical Assessment of Testes

Testes were embedded in paraffin wax after fixation in 4% paraformaldehyde, sectioned at 4-μm thickness, and stained with hematoxylin and eosin.[29] Light microscopy was used for routine observations. For immunohistochemical staining, the sections were incubated with 10% goat serum for 1 hour at room temperature, followed by incubation overnight at 4°C with a rabbit polyclonal antibody against ubiquitin (1:500; DakoCytomation, Glostrup, Denmark) or Nedd8 (1:500; Alexis Biochemicals, San Diego, CA) diluted in phosphate-buffered saline (PBS) containing 1% bovine serum albumin. Sections were then incubated with fluorescein isothiocyanate-conjugated goat anti-rabbit IgG (1:200; Jackson ImmunoResearch, West Grove, PA) for 1 hour at room temperature and examined by confocal laser-scanning microscopy (Olympus, Tokyo, Japan).

Apoptotic cells in testicular tissues were identified by terminal deoxynucleotidyl transferase (TdT)-mediated nick-end labeling (TUNEL) using the DeadEnd Fluorimetric TUNEL system kit (Promega, Madison, WI) and the anti-PARP p85 fragment pAb (Promega) according to the manufacturer's instructions.

Quantitative Analysis of Apoptotic Germ Cells

The number of apoptotic cells was determined by counting the positively stained nuclei in 30 circular seminiferous tubule cross-sections per testis section.[23,29] The proportion of seminiferous tubules containing apoptotic germ cells was calculated by dividing the number of seminiferous tubules containing apoptotic cells by the total number of seminiferous tubules. The incidence of apoptotic cells per apoptotic cell-containing seminiferous tubule was categorized into three groups, defined as 1 to 5, 6 to 10, and >11 positive cells.

Western Blotting

Western blots were performed as previously reported.[8,18,29] Total protein (5 μg/lane) was subjected to sodium dodecyl sulfate-polyacrylamide gel electrophoresis using 15% gels (Perfect NT Gel; DRC, Japan). Proteins were electrophoretically transferred to polyvinylidene difluoride membranes (Bio-Rad, Hercules, CA) and blocked with 5% nonfat milk in TBS-T [50 mmol/L Tris base, pH 7.5, 150 mmol/L NaCl, 0.1% (w/v) Tween-20]. The membranes were incubated individually with one or more primary antibodies to UCH-L1 and UCH-L3 (1:1000; peptide antibodies[18]), Bcl-2, Bcl-xL, Bax, p53, and caspase-3, (1:1000; all from Cell Signaling Technology, Beverly, MA), phosphorylated cyclic AMP response element-binding protein (pCREB, 1:500; Upstate Biotech-

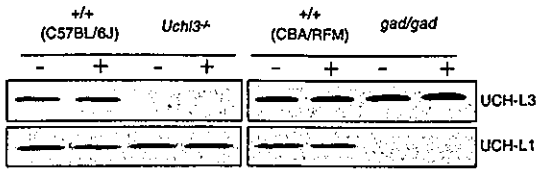

Figure 1. Western blotting analyses of both UCH-L3 and UCH-L1 in the testes of *gad* and *Uchl3* knockout mice, respectively, on day 4 after cryptorchid injury. Scrotal and cryptorchid testes did not differ significantly with respect to protein expression (−, scrotal testes; +, cryptorchid testes).

nology, Waltham, MA), brain-derived neurotrophic factor (BDNF, 1:500; Santa Cruz Biotechnology, Santa Cruz, CA), XIAP (1:500; Transduction Laboratories, Franklin Lakes, NJ), polyubiquitin (1:1000, clone FK-2; Medical & Biological Laboratories, Nagoya, Japan), monoubiquitin (1:1000, u5379; Sigma-Aldrich, St. Louis, MO), and Nedd8 (1:1000; Alexis Biochemicals, San Diego, CA). Blots were further incubated with peroxidase-conjugated goat anti-mouse IgG or goat anti-rabbit IgG (1:5000; Pierce, Rockford, IL) for 1 hour at room temperature. Immunoreactions were visualized using the SuperSignal West Dura extended duration substrate (Pierce) and analyzed with a Chemi-Imager (Alpha Innotech, San Leandro, CA). Each protein level was relatively quantificated after analysis with a ChemiImager using AlphaEase software.

Statistical Analysis

The mean and SD were calculated for all data (presented as mean ± SD). One-way analysis of variance was used for all statistical analyses.

Results

Level of Two UCH Isozymes in Scrotal and Cryptorchid Testes from Uchl3 Knockout and Gad Mice

We first confirmed the lack of UCH-L3 protein in the testes from *Uchl3* knockout mice by Western blotting (Figure 1). Similarly, we did not detect UCH-L1 protein in the testes of *gad* mice (Figure 1), as we previously observed.[13] Thus, in a biochemical sense, *gad* mice are analogous to *Uchl1*-null mice.[8,13] Compensatory level of UCH-L3 and UCH-L1 in *gad* and *Uchl3* knockout mice, respectively, was not observed (Figure 1; compare UCH-L3/UCH-L1 level with that of wild-type control mice). Experimental cryptorchidism did not affect UCH-L3 level in *gad* or wild-type control mice. Similarly, cryptorchidism did not affect UCH-L1 level in *Uchl3* knockout and wild-type control mice (Figure 1). Quantitative reverse transcriptase-polymerase chain reaction analysis showed that transcription from the *Uchl3* and *Uchl1* in both scrotal and cryptorchid testes from *gad* and *Uchl3* knockout mice was not significantly different from that measured in the corresponding wild-type control mice (data not shown). These results suggest that the level of UCH-L3 is regulated independently of UCH-L1 in the mouse testis,

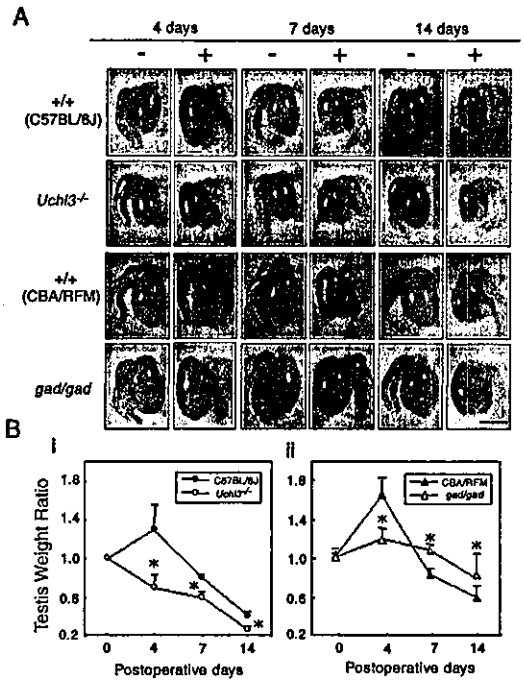

Figure 2. Comparison of testicular sizes and weights after experimental cryptorchidism. **A:** Gross images of changes in testicular size throughout time in two wild-type (C57BL/6J and CBA/RFM), *Uchl3* knockout, and *gad* mice (−, scrotal testes; +, cryptorchid testes). **B:** Ratio of cryptorchid to scrotal testis weight on days 0, 4, 7, and 14 after injury. i: Throughout time, the ratio for *Uchl3* knockout mice (**open circles**) differed significantly compared with wild-type mice (**filled circles**). ii: The ratio for *gad* mice (**open triangles**) did not differ significantly throughout time compared with wild-type mice (**closed triangles**). ($n = 4$; *, $P < 0.05$). Scale bar, 5 mm. Original magnifications, ×40.

and that cryptorchid injury does not affect the level of either protein.

Changes in Testicular Weight and Structure in Cryptorchid Uchl3 Knockout and Gad Mice

Unilateral cryptorchidism was surgically induced in *Uchl3* knockout and *gad* mice, and testes were evaluated on days 0, 4, 7, and 14 after the operation (Figure 2). Nonoperated (scrotal) testes served as controls for the evaluation of testicular weight and histochemistry. Cryptorchid testes from *Uchl3* knockout mice appeared smaller than the nonoperated controls at each time point, whereas the size of the cryptorchid testes from *gad* mice was similar to the controls (Figure 2A). Figure 2B shows the time course of the ratio of testicular weight of cryptorchid testes to scrotal testes. In wild-type mice (C57BL/6J and CBA/RFM), the ratio transiently increased 4 days after cryptorchid injury, most likely a consequence of inflammation-induced fluid accumulation[22,23] and biochemical changes observed. The ratio for these mice subsequently decreased below 1.0 by day 7. The ratio remained ~1.0 in *gad* mice (range,1.15 ~ 0.85), whereas it decreased significantly in *Uchl3* knockout mice compared with wild-type mice (Figure 2B). These results demonstrate that testes from *Uchl3* knockout and *gad* mice differ in their response to experimental cryptorchidism.

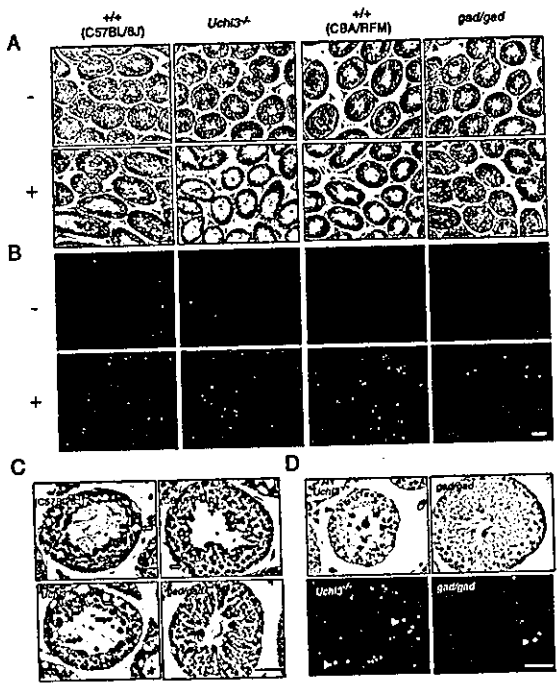

Figure 3. Histology and TUNEL staining of testicular cross sections after experimental cryptorchidism. **A:** Morphological analysis of seminiferous tubules on day 7 after cryptorchid injury. Note the germ cell loss and atrophy in cryptorchid testes compared with uninjured controls. (−, scrotal testes; +, cryptorchid testes). **B:** TUNEL staining of testicular cross-sections on day 7 after cryptorchid injury. Green fluorescence, TUNEL-positive cells; red fluorescence, nuclei stained with propidium iodide. **C:** Magnified cryptorchid testes sections. Pyknotic bodies (**filled arrows**) and Sertoli cell vacuolization (**open arrows**) were evident in cryptorchid testes of *Ucbl3* knockout and the two wild-type (C57BL/6J and CBA/RFM) mice on day 7 after injury. **D:** PARP analysis to detect apoptotic germ cells in cryptorchid testes of *Uchl3* knockout and *gad* mice on day 7 after injury. The detection of apoptotic germ cells (**arrowheads, top**) by PARP analysis was consistent with that of apoptotic germ cells (**arrowheads, bottom**) by TUNEL analysis. Scale bar, 50 μm. Original magnifications: **A** and **B** ×100; **C** and **D** ×200.

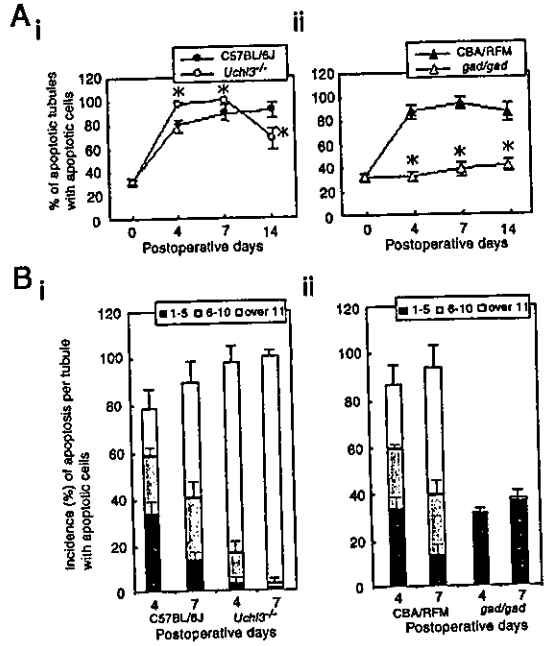

Figure 4. Quantitation of testicular germ cell apoptosis in testes after experimental cryptorchidism. **A:** The percentage of seminiferous tubules containing apoptotic germ cells in cryptorchid testes on days 0, 4, 7, and 14 after injury. **i:** The increase in the percentage of tubules containing apoptotic cells in the cryptorchid testes of *Ucbl3* knockout mice is statistically significant compared with wild-type mice on days 4, 7, and 14. Each value represents the mean ± SD; *, $P < 0.05$. **ii:** The percentage of apoptotic tubules in cryptorchid testes of *gad* mice is significantly different on days 4, 7, and 14 after injury. Each value represents the mean ± SD; *, $P < 0.01$. **B:** Incidence of apoptosis per seminiferous tubule with apoptotic germ cells on days 4 and 7 after injury. The incidence of seminiferous tubules containing >11 apoptotic germ cells is significantly increased ($P < 0.05$) in cryptorchid testes of *Ucbl3* knockout mice compared with wild-type mice. **i:** Comparison with *Ucbl3* knockout mice. **ii:** Comparison with *gad* mice. Each value represents the mean ± SD.

Testicular Germ Cell Apoptosis in Cryptorchid Uchl3 Knockout and Gad Mice

To explore the mechanism underlying the observed differences between *Uchl3* knockout and *gad* cryptorchid testes, we prepared histological cross-sections on day 7 after testicular injury (Figure 3, A and C). The presence of nuclear pyknosis, multinucleated giant cells, and Sertoli cell vacuolization with germ cell loss in the germinal epithelium is indicative of cryptorchid testes.[22,23] These hallmarks of testicular injury were the most remarkable characteristics of cryptorchid testes from *Uchl3* knockout mice, demonstrating profound testicular atrophy and germ cell loss compared with wild-type mice (Figure 3, A and C). In contrast, no nuclear pyknosis, cellular shrinkage, or germ cell loss was observed in cryptorchid testes from *gad* mice. Spermatocytes and early spermatids comprised the majority of affected cell types in cryptorchid testes (Figure 3, A and C).

Germ cell apoptosis was further examined by TUNEL and PARP assays in tissue sections from postoperative day 7 mice (Figure 3, B and D). All but the *gad* cryptorchid testes showed a time-dependent increase in germ cell apoptosis during experimental cryptorchidism; germ cell apoptosis was always found in tubules that had germ cell loss on days 4, 7, and 14 (Figure 3, B and D, and Figure 4). Compared to wild-type mice, the cryptorchid testes of *Uchl3* knockout mice showed a marked increase in apoptotic germ cells in response to testicular injury, whereas *gad* mice lacked cryptorchid-induced germ cell apoptosis (Figure 3B and Figure 4). By postoperative days 4 and 7, the percentage of seminiferous tubules containing apoptotic germ cells increased with statistical significance ($n = 4$) ($P < 0.05$) in cryptorchid testes of *Uchl3* knockout mice as compared with wild-type mice (Figure 4A). In addition, cryptorchid testes of *Uchl3* knockout mice showed a high incidence of seminiferous tubules containing >11 apoptotic germ cells on days 4 and 7 days as compared with wild-type mice (Figure 4B); however, germ cell apoptosis did not increase in cryptorchid testes of *gad* mice during postoperative days 4 to 14 ($P < 0.01$) (Figure 4, A and B).

Cellular Mono- and Polyubiquitin Level in Cryptorchid Uchl3 Knockout and Gad Mice

Ubiquitin is required for energy-dependent degradation of structurally altered proteins.[26] We previously reported that UCH-L1 binds ubiquitin and stabilizes ubiquitin turnover in neurons, and that the level of monoubiquitin is decreased in *gad* mice.[13] In a model of ischemic insult in the retina, ubiquitin induction was unexpectedly lower and ischemic

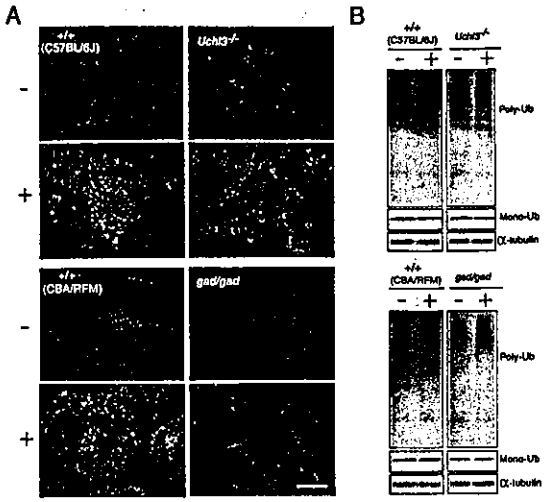

Figure 5. Immunohistochemical and Western blotting analyses of mono- and polyubiquitin in testes on day 7 after experimental cryptorchidism. **A:** Ubiquitin induction was not different between cryptorchid testes from *Uchl3* knockout and wild-type mice, whereas cryptorchid-induced ubiquitin induction in *gad* mice was reduced. Green fluorescence, ubiquitin-positive cells; red fluorescence, nuclei stained with propidium iodide. **B:** Polyubiquitin level in *Uchl3* knockout mice and the two wild-type (C57BL/6J and CBA/RFM) mice substantially increased after injury, whereas that in *gad* mice did not change significantly. Monoubiquitin level did not change after injury. Representative images from four independent experiments are shown (−, scrotal testes; +, cryptorchid testes). Scale bar, 50 μm. Original magnifications, ×200.

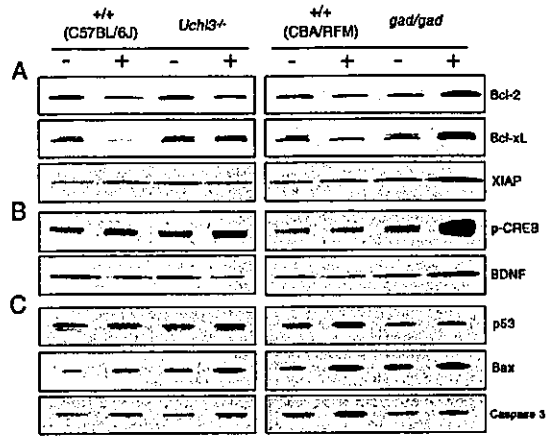

Figure 6. Western blotting analysis of anti-apoptotic, prosurvival, and apoptotic proteins in testes after experimental cryptorchidism. Total protein (5 μg per lane) was prepared from scrotal and cryptorchid testes on day 4 after cryptorchid injury. The expression levels of anti-apoptotic (**A**), prosurvival (**B**), and apoptotic (**C**) proteins in the cryptorchid testes of *Uchl3* knockout, *gad*, and the two wild-type (C57BL/6J and CBA/RFM) mice were significantly different compared with control mice. Representative images from four independent experiments are shown (−, scrotal testes; +, cryptorchid testes).

damage was weaker in the retina of *gad* mice (compared with wild-type mice) after ischemic insult.[17] To determine whether the increase in germ cell apoptosis in cryptorchid testes is associated with ubiquitin induction, we performed immunohistochemical analysis of testes from postoperative day 7 mice. Ubiquitin immunoreactivity increased substantially in cryptorchid testes from *Uchl3* knockout mice and the two wild-type mice, whereas those from *gad* mice showed only minor ubiquitin induction (Figure 5A). The scrotal testes of *Uchl3* knockout and *gad* mice did not show significant differences in ubiquitin induction compared with corresponding controls (Figure 5A). Interestingly, most of the increased ubiquitin induction was detected in spermatocytes and spermatids, consistent with the data on germ cell apoptosis after cryptorchid injury (Figure 3D and Figure 5A). Cryptorchid-induced polyubiquitin levels in the testes from *Uchl3* knockout and the two wild-type mice also increased substantially after injury, whereas the cryptorchid testes of *gad* mice showed no significant difference compared with scrotal testes (Figure 5B); however, the expression levels of monoubiquitin did not change significantly in any of the mice after cryptorchid injury.

Level of Anti-Apoptotic and Apoptotic Proteins in Cryptorchid Uchl3 Knockout and Gad Mice

We previously showed that anti-apoptotic proteins such as Bcl-2 and prosurvival proteins including phosphorylated cyclic AMP response element-binding protein (pCREB) are up-regulated in degenerated retina of *gad* mice.[17] These proteins are degraded by ubiquitination-mediated proteolysis.[30] We examined the expression of the Bcl-2 family proteins, XIAP, pCREB, and caspases to determine their role in testicular germ cell apoptosis after experimental cryptorchidism 4 days after injury in *Uchl3* knockout and *gad* mice. The level of anti-apoptotic proteins such as Bcl-2, Bcl-xL, and XIAP was up-regulated (323.8 ± 57.5, 262.3 ± 22.1, and 209.9 ± 11.7, respectively, as compared with wild type, 100) in the cryptorchid testes of *gad* mice compared with wild-type mice (Figure 6A). Additionally, pCREB, which is normally degraded in a ubiquitination-mediated manner,[30] was apparently highly up-regulated (259.0 ± 22.6, as compared with wild type, 100) in the cryptorchid testes of *gad* mice (Figure 6B). It has been demonstrated that pCREB activates genes that up-regulate trophic factors including BDNF.[31,32] Consistent with pCREB up-regulation, BDNF level also increased (203.0 ± 19.6, as compared with wild type, 100) in cryptorchid testes of *gad* mice (Figure 6B). Level was variable for anti-apoptotic, prosurvival, and apoptotic proteins in the cryptorchid testes of *Uchl3* knockout mice. The level of pCREB, p53, Bax, and caspase3 was slightly increased (169.9 ± 15.2, 152.6 ± 12.9, and 157.3 ± 14.0, respectively, as compared with scrotal testes, 100) in cryptorchid testes of *Uchl3* knockout mice compared with scrotal testes (Figure 6, B and C). Wild-type control mice had a similar expression level pattern except for pCREB. Because p53 acts as an upstream activator of Bax expression,[33] the observed Bax up-regulation after cryptorchid injury was consistent with the elevated p53 level in *Uchl3* knockout and wild-type control mice (Figure 6C). In contrast, BDNF was down-regulated (74.3 ± 7.7 as compared with wild type, 100) in cryptorchid testes of *Uchl3* knockout mice (Figure 6B). The down-regulation of BDNF combined with the up-regulation of pCREB suggests that BDNF might be regulated by another pathway that involves UCH-L3 but not pCREB.[34] Compared with scrotal testes, the expression of anti-apoptotic proteins decreased or was unchanged in cryptorchid testes of *Uchl3* knockout mice (Figure 6A).

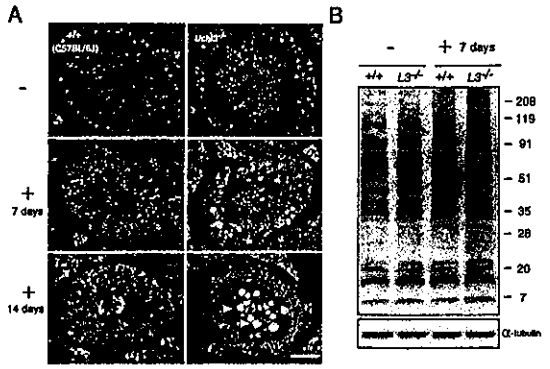

Figure 7. Immunohistochemical and Western blotting analyses of Nedd8 in testes from *Uchl3* knockout mice on days 7 and 14 after experimental cryptorchidism. **A:** Nedd8 induction in *Uchl3* knockout mice increased in both scrotal and cryptorchid testes. The shedding germ cells (**arrowheads**) in the cryptorchid testes of *Uchl3* knockout mice showed strong Nedd8 induction (−, scrotal testes; +7 days and + 4 days, cryptorchid testes). Green fluorescence, Nedd8-positive cells; red fluorescence, nuclei stained with propidium iodide. **B:** On day 7, the expression levels of Nedd8-conjugated proteins in *Uchl3* knockout mice were higher than in wild-type mice. Representative images of four independent experiments are shown. Scale bar, 50 μm. Original magnifications, ×200.

Nedd8 Level in Cryptorchid Uchl3 Knockout Mice

The varied expression levels of ubiquitin, anti-apoptotic, and apoptotic proteins in cryptorchid testes did not adequately explain the relatively exacerbated testicular atrophy and germ cell loss in *Uchl3* knockout mice compared with wild-type mice. We explored the underlying mechanism of this observation using the fact that UCH-L3 cleaves Nedd8.[14,16] We tested whether any change in Nedd8 expression correlated with greater testicular atrophy and germ cell loss in *Uchl3* knockout mice. Nedd8 immunoreactivity was highly detected in scrotal and cryptorchid testes from *Uchl3* knockout mice compared with wild-type mice (Figure 7A). The increased Nedd8 induction was mainly observed in spermatocytes and spermatids, and its expression pattern was similar to that of UCH-L3 during spermatogenesis.[18] These results suggest that Nedd8 may interact closely with UCH-L3 during testicular atrophy and germ cell loss. The cryptorchid testes of *Uchl3* knockout mice showed time-dependent and rapid Nedd8 induction compared with wild-type mice throughout the period 7 to 14 days after injury (Figure 7A). Moreover, the cryptorchid testes of *Uchl3* knockout mice showed strong Nedd8 induction in luminal shedding germ cells on day 14. An immunoblot of scrotal and cryptorchid testes proteins on day 7 confirmed the higher expression levels of Nedd8-conjugated proteins in *Uchl3* knockout mice as compared with wild-type mice (Figure 7B).

Discussion

During spermatogenesis, apoptosis controls germ cell numbers and eliminates defective germ cells to facilitate testicular homeostasis.[35–37] Recent studies indicate that ubiquitination targets proteins for degradation and modulates the turnover of various classes of short-lived signaling proteins.[28,38] Germ cell apoptosis after cryptorchid stress involves genes for various factors, such as Bcl-2 family proteins, p53, and caspases;[39–44] however, the impact of the ubiquitin system on the regulatory mechanisms of germ cell apoptosis is not fully understood. In a previous study, we used *gad* mice, which lack UCH-L1 expression, to show that neural cell apoptosis is suppressed after ischemic retinal injury *in vivo*.[17] These results suggest that UCH-L1 is involved in apoptosis-inducing pathways after stress. UCH-L1 and UCH-L3 are highly similar in sequence; however, UCH-L3 is expressed ubiquitously,[7] whereas UCH-L1 is selectively expressed in neurons and testes/ovaries.[8,9] We recently demonstrated that the expression of these UCH isozymes is differentially and developmentally regulated during spermatogenesis, and that UCH-L1 and UCH-L3 likely have distinct functions during different developmental phases.[18]

To understand the pathophysiological roles of UCH-L1 and UCH-L3 *in vivo*, two mutant mice, *Uchl3* knockout and *gad* mice, were examined after cryptorchid injury. The cryptorchid testes of the two mutant mice had fundamental differences after injury, in that testes of *Uchl3* knockout mice showed profound apoptosis-mediated germ cell loss, whereas *gad* mice were relatively resistant to injury (Figures 3 and 4). In addition, cryptorchid testes of *Uchl3* knockout mice showed greater testicular atrophy and germ cell loss than wild-type mice.

There are several proposed mechanisms for germ cell loss after experimental cryptorchidism.[21–23,45] The tumor suppressor protein, p53, is highly expressed in the testis and regulates both cell proliferation and apoptosis.[23,28,37] A role for p53 in experimental cryptorchidism has been demonstrated convincingly. The higher temperature of the testis caused by cryptorchidism induces p53-mediated apoptosis in the testis, and p53 overexpression results in increased germ cell apoptosis and decreased spermatozoa production.[23,46] In addition to p53, the Bcl-2 family and IAP (inhibitor of apoptosis protein) family are other major classes of intracellular apoptosis regulators.[47,48] The Bcl-2 family can be divided into anti-apoptotic members, such as Bcl-2, Bcl-xL, and Bcl-w, and proapoptotic members, such as Bax and Bak.[49] It has been suggested that the ratio of proapoptotic to anti-apoptotic Bcl-2 family members is important in determining whether a cell will undergo apoptosis.[49] A major function of the Bcl-2 family members appears to be the regulation of mitochondrial events, such as the release of proapoptotic factors.[50] The IAP family inhibits apoptosis primarily by inactivating and degrading proapoptotic proteins.[51] XIAP, a member of IAP family, can bind to and inhibit the proteinase activity of cellular caspase-3 and caspase-9, and thereby block the apoptotic process.[44,52,53]

With regard to cryptorchid injury, the balance between the expression of apoptosis-inducing and apoptosis-protecting proteins constitutes one possible mechanism underlying the observed germ cell apoptosis and protection from apoptosis in *Uchl3* knockout and *gad* mice, respectively. In *gad* mice, cryptorchid injury caused a large increase in the anti-apoptotic proteins Bcl-2, Bcl-xL, and XIAP, consistent with our previous report using retina.[17]